



Petrology, geothermobarometry and geochemistry of granulite facies wall rocks and hosting gneiss of gemstone deposits from the Mogok area (Myanmar)

Myint Myat Phyto^{a,c}, Leander Franz^{a,*}, Rolf L. Romer^b, Christian de Capitani^a, Walter A. Balmer^c, Michael S. Krzemnicki^{a,c}

^a Department of Environmental Sciences, Mineralogy and Petrology, University of Basel, Bernoullistrasse 30, CH-4056 Basel, Switzerland

^b GFZ German Research Centre for Geosciences, Telegrafenberg, D-14473 Potsdam, Germany

^c Swiss Gemmological Institute SSEF, Aeschengraben 26, CH-4051 Basel, Switzerland

ARTICLE INFO

Keywords:

Mogok Metamorphic Belt
Granulite facies metamorphism
Garnet-nepheline gneiss
Subduction-related magmatism
Spinel-ruby gem deposit

ABSTRACT

The Mogok Metamorphic Belt (MMB) of Myanmar formed during the Paleogene collision between the West Burma block and the Shan-Thai block. The MMB is mainly composed of medium to high-grade metamorphic marble, calc-silicate rocks, gneiss, quartzite, peridotite and igneous rocks such as granite, syenite and gabbro. The Mogok area in the central part of the MMB is well-known for magnificent quality ruby, spinel, sapphire, and peridot. To unravel the metamorphic PT-conditions prevailing during the formation of spinel and ruby from primary marble deposits in the Mogok area, three different types of high-grade quartz-garnet gneiss from the neighbourhood of gemstone mines were investigated by electron microprobe. Geothermobarometry reveals granulite facies PT-conditions of 756–792 °C at 7.4–7.6 kbar, which is reproduced by Theriak-Domino modelling within the error of both methods at water activities of 0.34–0.4. Shoshonitic and high-K calc-alkaline mafic dykes occur within marble forming conspicuous garnet-nepheline and clinopyroxene-clinoamphibole gneiss. Petrologic and geochemical investigations of these metadykes verify their granulite facies metamorphism and classify them as subduction-related magmatic rocks, which intruded the marble sequences. These investigations as well as previous studies show that spinel and ruby in marble of the Mogok area may have formed not only by metasomatism around alkaline intrusions, but also by granulite facies regional metamorphism.

1. Introduction

Myanmar is well known for numerous deposits of world class precious gemstones. The Mogok area, also known as the Mogok stone tract, hosts the most important gemstone deposits in Myanmar (Iyer, 1953). Since the 15th century, this area is a major source of finest quality ruby, spinel and other gemstones (Iyer, 1953; Hughes, 1997).

In two previous studies we investigated ruby and spinel, which formed in marble and calc-silicate rocks of the Mogok Stone Tract. We found numerous high-grade mineral inclusions in spinel giving evidence for granulite-facies metamorphism (Phyo et al., 2019). Dating of zircon and zirconolite inclusions in spinel and ruby testified to the formation of the gemstones in Oligocene to Early Miocene time (Phyo et al., 2020). The present study is aiming to derive consistent PT-conditions of metamorphism and obtaining fluid conditions during the granulite

facies metamorphism, which led to the blastesis of the gemstones. As the thermobarometry of the ruby- and spinel-bearing marble was hampered by the absence of suitable mineral assemblages, we chose three types of high-grade quartz-garnet gneiss from the vicinity of gem deposits Aunglan Taung, Bawpadan, Yadanar Kaday Kadar and Kinn in the central and western part of the Mogok area. Furthermore, we investigated mafic dykes and layers occurring in several deposits intercalated with the gemstone-bearing marble, now forming unique nepheline- and clinopyroxene-clinoamphibole gneiss. Here, the aim was to further examine their composition and to define the metamorphic grade these rocks experienced in order to investigate their possible influence on the formation of the gemstones.

* Corresponding author at: Department of Environmental Sciences, Quaternary Geology, University of Basel, Basel, 4056, Switzerland.

E-mail address: leander.franz@unibas.ch (L. Franz).

<https://doi.org/10.1016/j.jaesx.2022.100132>

Received 5 October 2022; Received in revised form 1 December 2022; Accepted 3 December 2022

Available online 7 December 2022

2590-0560/© 2022 The Author(s). Published by Elsevier Ltd. This is an open access article under the CC BY license (<http://creativecommons.org/licenses/by/4.0/>).

2. General geology

The recent tectonic history of Myanmar is dominated by the Cenozoic closure of the Neotethys, but the involved tectonic blocks are much older, had separated – starting in the Paleozoic – from Gondwana and were accreted to growing Asia by the closure of various branches of the Tethys ocean (e.g., Metcalfe, 2013).

From the Triassic, the western margin of the Shan-Thai block (also referred to as Sibumasu) developed into an active margin with increasingly younger sutures from the east to the west (Gardiner et al., 2014). Eastward subduction beneath the Shan-Thai block resulted in the formation of several belts of late Triassic and younger granite (Gardiner et al., 2014), and the metasomatism of the lithospheric mantle beneath

the Shan-Thai block by subducted sedimentary rocks. The closure of the Neotethys preceding the collision of India with Asia resulted in the Paleogene collision of the West Burma block with the Shan-Thai block and the continued subduction of the Indian plate beneath the West Burma block (Searle and Haq, 1964; Searle et al., 2007, 2017, cf. Fig. 1).

The Shan-Thai block includes two crustal domains, the Slate Belt to the east and the Mogok Metamorphic Belt (MMB) to the west, the latter extending over 1500 km from the Himalayan Syntaxis in the north to the Andaman Sea in the south (cf. Chhibber, 1934; Fennor, 1930; La Touche, 1913; see Fig. 1). The Slate Belt is dominated by Carboniferous to early Permian clastic sediments that have experienced low-grade metamorphism and were intruded by I-type and S-type granite (Gardiner et al., 2014). In contrast, the MMB is mainly composed of

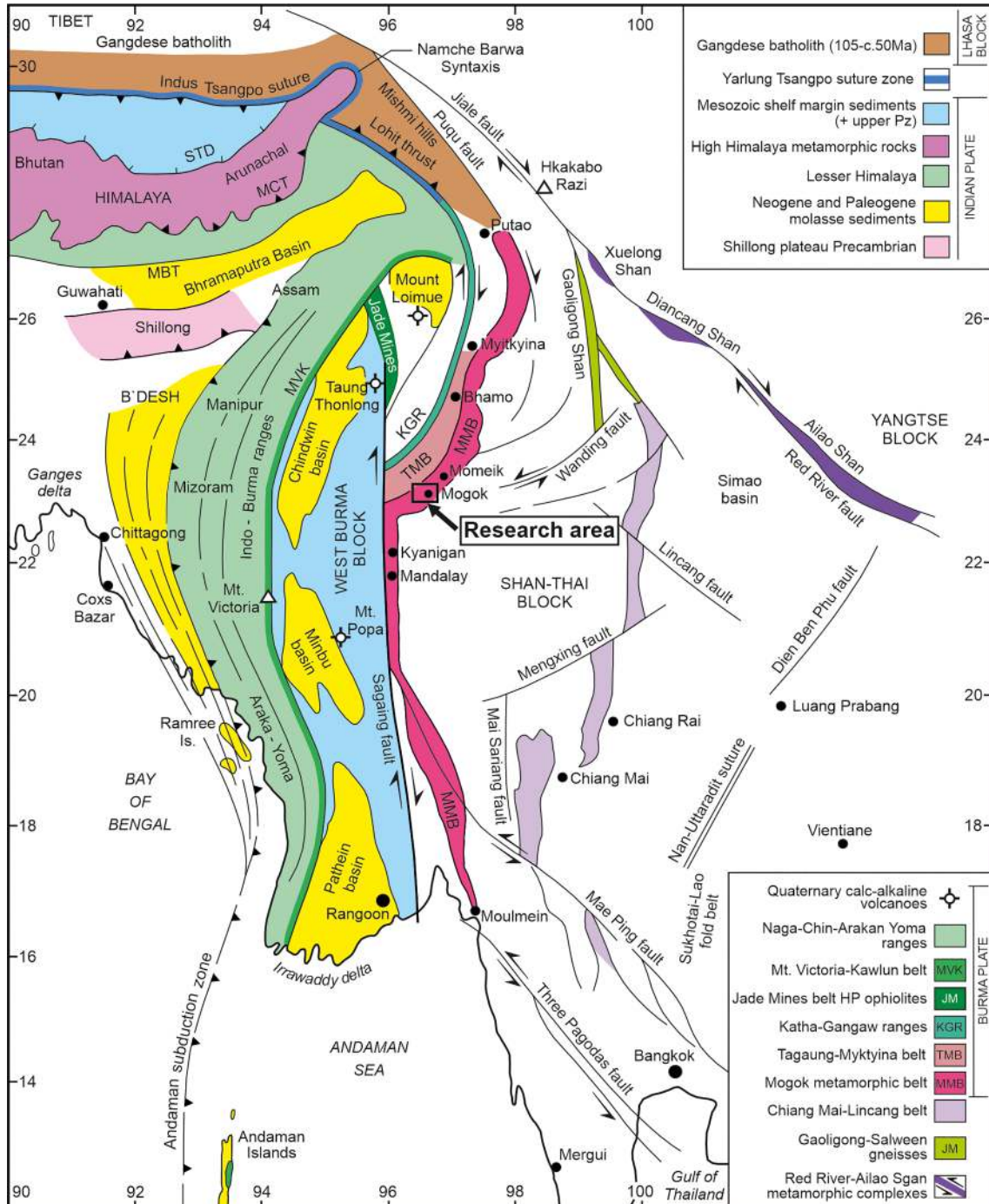


Fig. 1. Geological map of SE Asia, Myanmar, and the Andaman Sea showing the major structural features and terrane boundaries (modified after Searle et al., 2007).

medium to high-grade metamorphic rocks such as marble, calc-silicate rock, gneiss and peridotite and igneous rocks such as granite, charnockite, syenite and gabbro.

The latest, high-grade regional metamorphic event in the MMB occurred in the Paleogene to Early Neogene due to the collision of the Shan-Thai block with the West Burma Block (Fig. 1) subsequent to the collision of the Indian and Asian plates (Dewey et al., 1989, Sone and Metcalfe, 2008, Zaw et al., 2017, Searle et al., 2017).

Both the Slate Belt and the MMB were intruded by Late Cretaceous and younger granite (Gardiner et al., 2015), as well as mafic dikes and syenite (Barley et al., 2003; Thu, 2007). In the MMB, Triassic and Cretaceous intrusions and their sedimentary host rocks were overprinted by Paleogene medium pressure, medium-high temperature metamorphism. Late Paleogene and Neogene intrusions post-date metamorphism (Bender, 1983; Zaw, 1989, 1990, 2017; Zaw et al., 2015).

The Mogok area in the central part of the MMB is made up of gneiss, marble, calc-silicate rock, peridotite and quartzite that have been intruded by felsic, mafic and alkaline igneous rocks (Iyer, 1953; Searle et al., 2020). A foliated augite-biotite granite northwest of Mogok shows Cretaceous zircon ages of 129.8 ± 8.2 Ma, whereas a syenite close to Mogok yields zircon rim ages of 30–45 Ma, which was interpreted to mirror the Paleogene metamorphic overprint (Thu, 2007). Zircon and titanite ages of charnockite and syenite fall into three age groups, i.e. Jurassic (170–168 Ma), Palaeocene (68–63 Ma) and Eocene-Oligocene (44–21 Ma; Searle et al., 2020). Post-tectonic biotite granite intrusions, also known as Kabaing granite, were dated at 16 Ma (Searle and Haq, 1964). These rocks are widely distributed in the western part of the Mogok area (Fig. 2) and extend to the Thabeikkyin area in the West (Themelis, 2008; Thu, 2007; Waltham, 1999; Zaw, 1990, 1998). Earlier studies on the Mogok area either focused on gemmology (Brown & Judd,

1896; Fermor, 1930; Chhibber, 1934; Gübelin & Koivula, 1986, 2005; Giuliani et al., 2005, 2015, 2017; Themelis, 2008, Hughes et al., 2014, 2017) or on the tectonic development of the region by using regional geology, geochemistry, geochronology and geothermobarometry (Bertrand et al., 1999, 2001; Garnier et al., 2006, 2008; Mitchell, 1993; Zaw et al., 2010; Sutherland et al., 2019). Only in recent years, research on the Mogok and adjacent areas increasingly investigated the genesis of the gem deposits in the context of their host rocks and their tectonic development (Htay et al., 2017; Searle et al., 2007, 2020; Thu, 2007; Thu et al., 2017; Win et al., 2016; Yonemura et al., 2013).

Investigations of metamorphism in of the MMB demonstrate that the rocks reached amphibolite to granulite facies conditions and the metamorphic grade increases from the east to the west (Thu et al., 2017). Maximum PT- conditions of 780–860 °C at 6.0–8.4 kbar in the Ozone and Thabeikkyin areas to the west of Mogok are close to those obtained a garnet-orthopyroxene granulite from the Mogok area (800–950 °C at 6.5–7.8 kbar; Yonemura et al., 2013). Htay et al. (2017) reported PT-conditions of > 840 °C at > 3.5 kbar for a sillimanite-garnet gneiss and 770–840 °C at 2.2–3.5 kbar for a migmatite from the Momeik area northeast of Mogok (Fig. 1) and also described polymetamorphism in these low- to medium-pressure granulites. Similar PT-conditions of 780–850 °C at 6.0–10.0 kbar on a granulite facies paragneiss were reported from the Sagaing area to the west of Mandalay (Win et al., 2016), whereas upper amphibolite facies PT-conditions of 680 °C at 4.5 ± 1.7 kbar have been determined for a granitic gneiss from the Kyanigan quarry to the north of Mandalay (Fig. 1; Searle et al., 2007).

3. Sample material and analytical methods

Petrologic and geothermobarometric investigations were performed

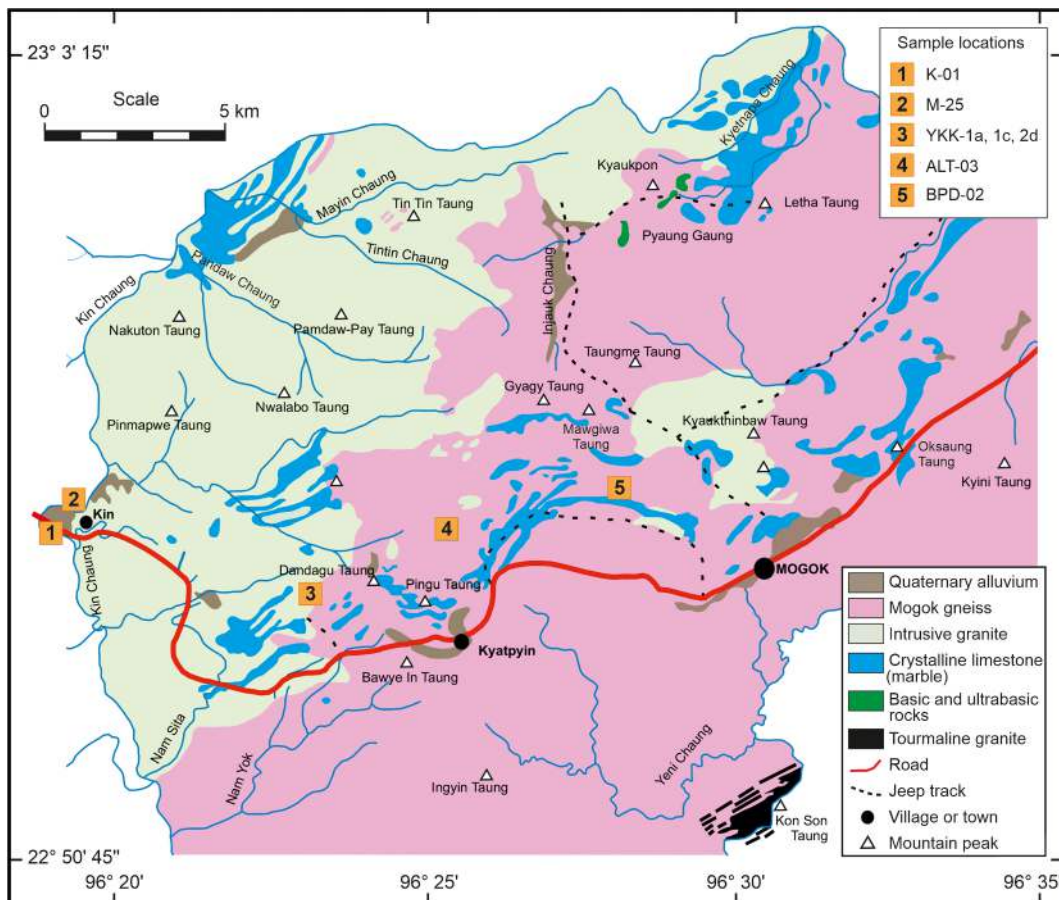


Fig. 2. Geological map of the Mogok area (modified after Iyer, 1953) showing the locations of the investigated samples.

on a biotite-garnet-orthopyroxene gneiss (ALT-03), a sillimanite-bearing biotite-garnet gneiss (BPD-02), a biotite-garnet gneiss (K-01), three types of petrographically different garnet-clinopyroxene-nepheline gneiss (YKK-1a; YKK-1c; M-25) and one clinopyroxene-amphibole gneiss (YKK-2d) from the central and the Western part of the Mogok area (see Fig. 2). Biotite-garnet-orthopyroxene gneiss sample ALT-03 originates from a road outcrop north of Pingu Taung (Fig. 3a) at the slope of the Aung Lan Mountain. The gneiss is framed by a syenite intrusion at the foot of the mountain and by spinel-bearing marble and granite at the top of the mountain. Sillimanite-garnet gneiss sample BPD-02 forms the wall rock of spinel- and ruby-bearing marble in Block



Fig. 3. Photos of outcrops in the western and central part of the Mogok Belt; a.) Outcrop of garnet-orthopyroxene gneiss ALT-03 showing a monotonous succession of thoroughly foliated gneiss, b.) Outcrop of sample K-01 displays microfolded garnet gneiss with irregularly alternating quartz- and garnet-biotite-rich layers, c.) Outcrop of nepheline gneiss M-25, which formed part of a massive metadyke with a thickness of 1.5–2 m. The neighbouring calcisilicate rocks are not exposed.

1 of the *gem* mine Bawpadan in the central part of the Mogok area. Garnet-biotite gneiss K-01 was collected from an outcrop at the main road near the village of Kin (Fig. 3b). The paragneiss, which is locally termed Mogok gneiss, is interbedded with lenticular layers of graphite and bands of marble. Close to outcrop K-01, garnet-clinopyroxene-nepheline gneiss sample M-25 was sampled from an outcrop on a hill. It was part of a small dyke, which intruded calcisilicate rocks (Fig. 3c). Garnet-clinopyroxene-kalifeldspar-nepheline gneiss YKK-1a and garnet-clinopyroxene-plagioclase-nepheline gneiss YKK-1c as well as clinopyroxene-amphibole gneiss YKK-2d were collected from a metadyke cutting through marble of the *gem* deposit Yadanar Kaday Kadar (Fig. 4h). Mineral assemblages of rock samples are shown in Table 1, mineral abbreviations follow Kretz (1983) and Spear (1993). Selected electron microprobe analyses of the minerals are listed in Tables S1–S8 of the electronic supplement.

4. Results

4.1. Petrography and mineral chemistry

4.1.1. Samples from the central part of Mogok

Sample ALT-03 is a fine-grained biotite-garnet-orthopyroxene gneiss, which shows cm-sized, alternating leucocratic layers rich in quartz and feldspar and layers enriched in biotite, orthopyroxene and garnet (Fig. 4a). Both layers display a granoblastic texture with a slight foliation by aligned biotite flakes. Main minerals are quartz, perthitic K-feldspar, plagioclase, biotite, orthopyroxene and garnet, whereas accessory minerals are ilmenite, zircon and apatite. Garnet has a pinkish colour and often shows elongate and irregular shapes with inclusions of quartz, orthopyroxene and plagioclase (Fig. 5a & b). A retrograde mineral assemblage formed around the garnet rim consisting of an inner layer of Na-rich plagioclase (albite/oligoclase) and an outer layer of carbonate (rhodochrosite), which is partly associated with limonite. Carbonate is also found on fractures in garnet. Electron microprobe analyses of the garnet reveal a slight increase of almandine at the expense of grossular from core ($\text{Alm}_{71.6}\text{Prp}_{11.2}\text{Sp}_{5.3}\text{UGA}_{12.0}$) to rim ($\text{Alm}_{74.1}\text{Prp}_{11.4}\text{Sp}_{5.5}\text{UGA}_{9.1}$). Orthopyroxene forms granoblastic and irregular grains with a faintly brownish colour and a rather constant composition of $\text{En}_{33.5-34.6}\text{Fs}_{64.4-65.2}\text{Wo}_{1.0-1.3}$. Reddish brown biotite has elevated TiO_2 contents of 5.8–6.3 wt-% and an X_{Mg} of 0.396–0.412. Plagioclase is unzoned with an average composition of $\text{Ab}_{72.2}\text{An}_{25.6}\text{Or}_{2.2}$ whereas perthitic K-feldspar shows a somewhat variable composition of $\text{Or}_{66-71.7}\text{Ab}_{27.3-34}\text{An}_{0-2.6}$. Electron microprobe analyses of sample ALT-03 are listed in Tables S1–S5 of the electronic supplement.

Sample BPD-02 is a fine- to medium-grained sillimanite-bearing biotite-garnet gneiss, showing several cm-wide, more and less leucocratic layers with homogeneously interspersed red garnet porphyroblasts (Fig. 4b). Under the microscope, a weak main foliation is visible, formed by elongate quartz and feldspar grains and by biotite flakes aligned parallel to the layering. Main minerals are quartz, perthitic K-feldspar, plagioclase, garnet and subordinate biotite. Sillimanite occurs as inclusions in garnet (Fig. 5c & d) and only rarely in the matrix. Ilmenite, apatite and zircon are accessory. There are numerous myrmekites at plagioclase-K-feldspar grain boundaries. Pale red garnet porphyroblasts show a flat zonation profile with slight, irregular variations of the composition ($\text{Alm}_{55.1-65.0}\text{Prp}_{38.1-38.9}\text{Sp}_{2.1-2.8}\text{UGA}_{3.1-3.8}$). Orangy red biotite flakes have high TiO_2 -contents of 7.3–8.3 wt-% and X_{Mg} -values of 0.58–0.62. Plagioclase is virtually unzoned with an average composition of $\text{Ab}_{76.6}\text{An}_{21.9}\text{Or}_{1.5}$ while perthitic K-feldspar has an average composition of $\text{Or}_{66.9}\text{Ab}_{30.52}\text{An}_{2.4}\text{Cs}_{0.2}$. Electron microprobe analyses of sample BPD-02 are listed in Tables S1, S2, S4 and S5 of the electronic supplement.

4.1.2. Samples from the western part of Mogok

Sample K-01 is a porphyroblastic biotite-garnet gneiss from the westernmost part of the MMB near the village of Kin and shows cm-

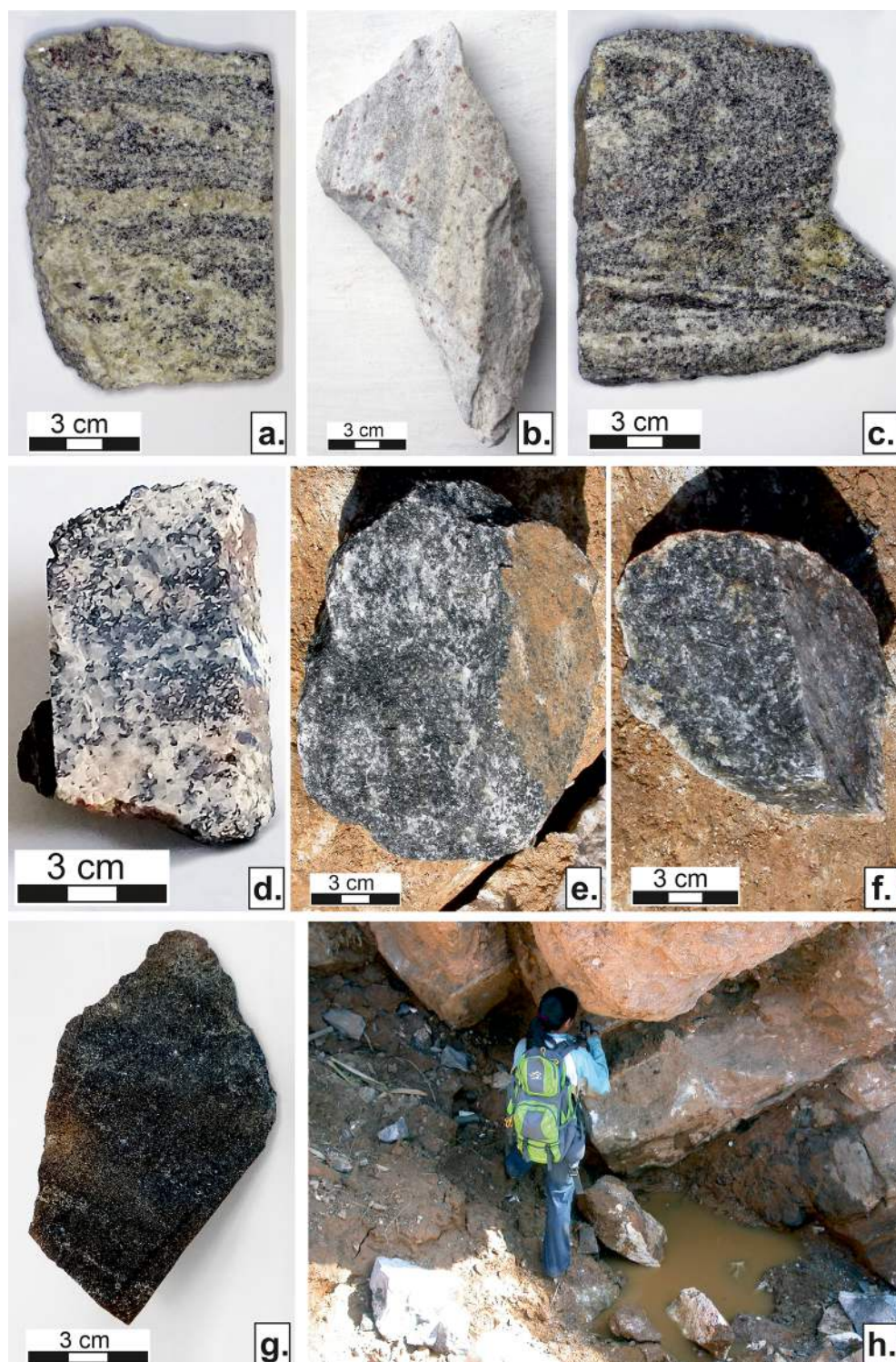


Fig. 4. Photos of hand specimens of the investigated samples and the outcrop of the metadyke; a.) Sample ALT-03: biotite-garnet-orthopyroxene gneiss, b.) Sample BPD-02: sillimanite-bearing biotite-garnet gneiss, c.) Sample K-01: biotite-garnet gneiss, d.) Sample M-25: carbonate-garnet-K-feldspar-clinopyroxene-nepheline gneiss, e.) Sample YKK-1a: carbonate-bearing garnet-K-feldspar-clinopyroxene-nepheline gneiss, f.) Sample YKK-1c: carbonate-bearing scapolite-garnet-plagioclase-clinopyroxene-nepheline gneiss, g.) Sample YKK-2d: clinopyroxene-clinoamphibole gneiss, h.) Open pit of the gem deposit Yadanar Kaday Kadar (YKK) with spinel- and ruby-bearing marble (pale brown) and metadyke (dark grey). The metadyke has a thickness of about 2 m.

sized, irregular microfolds (Fig. 4c). The matrix is fine-grained with aligned biotite flakes, elongate quartz and feldspar grains as well as interspersed porphyroblastic garnet crystals. Main minerals are quartz, K-feldspar, plagioclase, biotite, garnet and accessory apatite, zircon and pyrite. Poikiloblastic, pale red garnet has diameters up to 7 mm and often contains numerous rounded quartz inclusions (Fig. 5e & f). Electron microprobe analyses reveal an absence of zonation with rather constant compositions of $\text{Alm}_{59.1-61.9}\text{Prp}_{29.5-32.4}\text{Sps}_{1.8-2.9}\text{UGa}_{6.1-7.9}$ in all investigated garnet grains. Biotite shows TiO_2 -contents of 4.4–5.0 wt-% and X_{Mg} -values of 0.59–0.60. Plagioclase reveals slightly irregular

variations in composition from grain to grain ($\text{Ab}_{55.9-58.3}\text{An}_{39.9-41.9}\text{Or}_{1.3-2.3}$), which is also the case for K-feldspar ($\text{Or}_{87.4-87.9}\text{Ab}_{11.2-13.3}\text{An}_{07.1-4}\text{Cs}_{0-1.6}$). Electron microprobe analyses of sample K-01 are listed in Tables S1, S2, S4 and S5 of the electronic supplement.

Sample M-25, which originates from the vicinity of sample K-01 near the village of Kin, is part of a mafic layer within a calcisilicate marble. The medium-grained rock shows a somewhat inhomogeneous texture with mafic and felsic mineral accumulations (Fig. 4d). Under the microscope, the carbonate-garnet-K-feldspar-clinopyroxene-nepheline gneiss reveals a granoblastic texture with randomly oriented minerals.

Table 1
Mineral assemblages found in metamorphic rocks from the Mogok area; mineral abbreviations after Kretz (1983) and Spear (1993).

Sample	Location	Grt	Bt	Pl	Kfs	Opx	Cpx	Ne	Amp	Scp	Qtz	Ilm	Mag	Py	Zrn	Sil	Cc	Ttn
ALT-03	22° 55' 32.30" N 96° 25' 34.54" E	+	+	+	+	+	-	-	-	-	+	+	-	-	+	-	-	-
BPD-02	22° 56' 5.31" N 96° 27' 22.16" E	+	+	+	+	-	-	-	-	-	+	+	-	-	+	+	-	-
K-01	22° 55' 49.06" N 96° 19' 6.99" E	+	+	+	+	-	-	-	-	-	+	-	-	-	+	-	-	-
M-25	22° 56' 50.00" N 96° 19' 22.52" E	+	-	-	+	-	+	+	-	-	-	-	+	-	-	-	+	+
YKK-1a	22° 54' 42.14" N 96° 23' 17.35" E	+	-	-	+	-	+	+	-	-	-	-	+	+	-	-	+	+
YKK-1c	22° 54' 42.14" N 96° 23' 17.35" E	+	-	+	-	-	+	+	-	+	-	-	-	+	+	-	+	+
YKK-2d	22° 54' 42.14" N 96° 23' 17.35" E	-	-	+	-	-	+	-	+	-	-	-	-	+	-	-	-	+

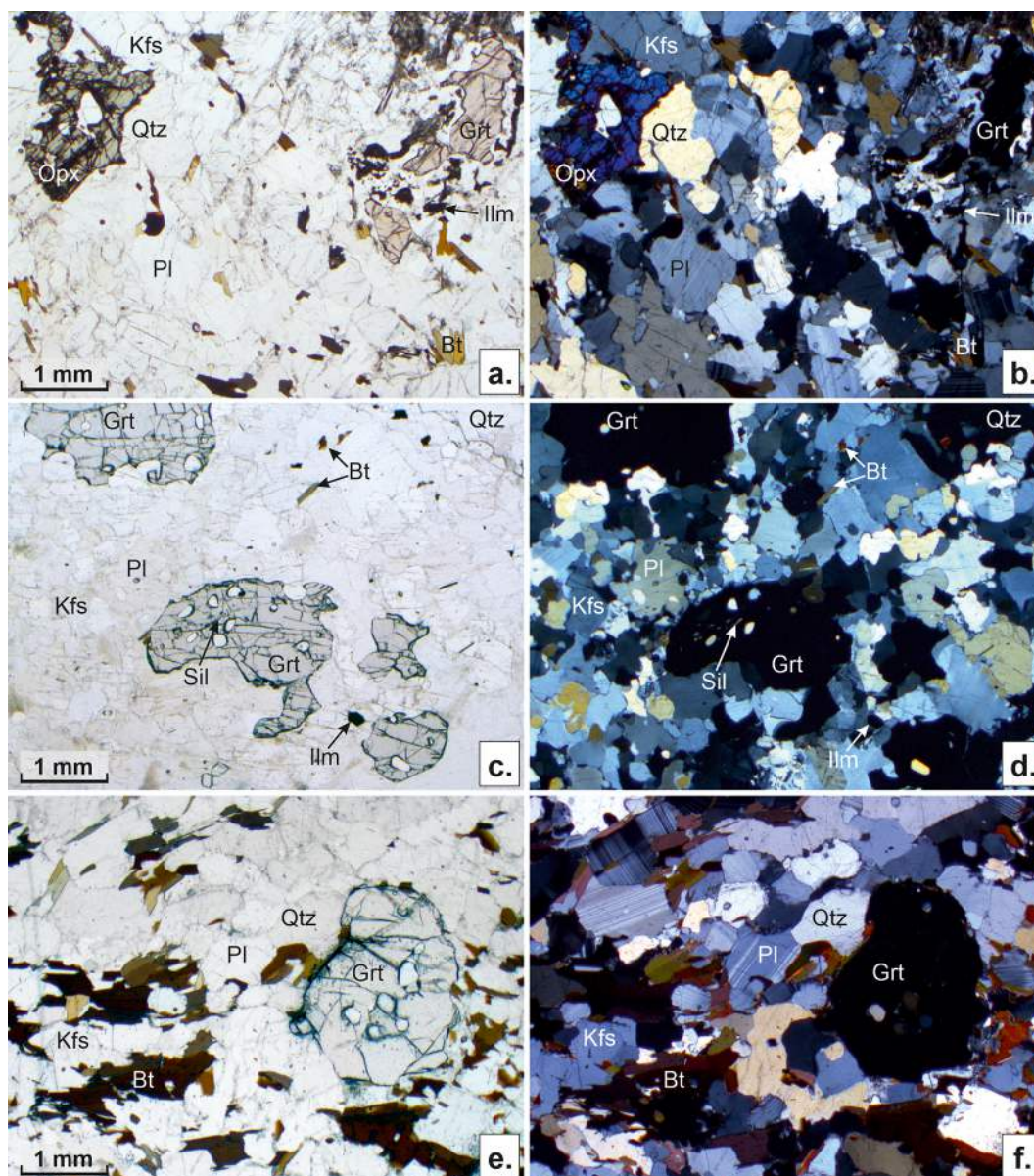


Fig. 5. Photomicrographs of the different types of quartz gneiss (parallel polarizers on the left side, crossed polarizers on the right side). a. and b.) sample ALT-03 showing a granoblastic fabric with the peak metamorphic assemblage Grt-Opx-Bt-Kfs-Pl-Qtz. Note the corona of carbonate and plagioclase around the garnet in the upper right corner c. and d.) sample BPD-02 is rich in Kfs, Pl, Qtz and Grt while Bt is rare and Sil only appears as tiny inclusions in Grt. e. and f.) sample K-01 contains porphyroblastic Grt, Bt flakes and granoblastic Kfs, Pl and Qtz.

In the mafic sections, aggregates of green clinopyroxene and poikiloblastic garnet are found while felsic sections show granular K-feldspar and nepheline (Fig. 6a & b). There are subordinate accumulations of carbonate and accessory amounts of apatite, titanite and magnetite. Electron microprobe analyses of yellowish brown garnet reveal elevated Ca- and Fe-contents with a composition of $\text{Alm}_{7.6-10.6}\text{Prp}_{0.9-1.2}\text{Sps}_{0.9-1.8}\text{Uv}_{0-0.3}\text{Gr}_{51.9-58.9}\text{Adr}_{28.0-37.0}$. TiO_2 contents of 1.4–1.8 wt-% are conspicuous. Compositional variations occur from grain to grain whereas zoning is not present. Clinopyroxene is identified by electron microprobe analyses as aegirine-rich augite following the classification of Morimoto et al. (1988) with a composition of $\text{Q}(=\text{En} + \text{Fs} + \text{Wo})_{81.5-86.7}\text{Aeg}_{12.7-16.6}\text{Jd}_{0.5-2.3}$ and minor variation from grain to grain. Nepheline was calculated on a base of 32 oxygens, which typically revealed more silicon and less aluminium than is represented by the formula (Deer et al., 1992, 2004) with Si contents of 8.283–8.508 p.f.u. An elevated K-content is indicated by X_K -values ($=\text{K}/(\text{K} + \text{Na} + \text{Ca})$) of 0.168–0.183. K-feldspar shows a variable composition from grain to grain with $\text{Or}_{73.3-75.4}\text{Ab}_{22.4-24.6}\text{An}_{1.3-1.8}\text{Cs}_{0.5-1.1}$. Carbonate is almost pure calcite with a CaCO_3 -content of > 99 mol-%. Electron microprobe analyses of sample BPD-02 are listed in Tables S1, S3, S5 and S6 of in the electronic data supplement.

Samples YKK-1a, YKK-1c and YKK-2d originate from different sections of a m-wide mafic layer within a calcisilicate marble succession at the ruby mine Yadanar Kaday Kadar near Kyauk Pyat That (Fig. 4h). The structure of this layer and its appearance within the metasedimentary unit strongly remind of a magmatic dyke. Sample YKK-1a, a medium-grained mafic gneiss with patchy felsic sections (Fig. 4e), originates from the central part of the layer and resembles to the nepheline gneiss M-25 concerning its mineralogy and rock fabric. Based on its mineral assemblage, the rock is a carbonate-bearing garnet-K-feldspar clinopyroxene-nepheline gneiss. Under the microscope, it shows a random orientation of granoblastic nepheline and K-feldspar as well as irregular intergrowths of garnet and clinopyroxene (Fig. 6c & d). Accessory minerals are calcite, apatite, titanite and magnetite, which is in part mantled by pyrite. Garnet shows reddish brown core and dark brown rim sections, with the latter often displaying irregularly lobate and symplectitic shapes. The rim sections of the garnet are always intergrown with nepheline while other phases are absent. Electron microprobe analyses testify to rather constant compositions of the reddish brown central garnet sections with $\text{Alm}_{6.8-10.1}\text{Prp}_{0.2-0.5}\text{Sps}_{1.3-2.4}\text{Uv}_{0-0.3}\text{Gr}_{38.1-42.2}\text{Adr}_{47.3-50.6}$ while the dark brown rim sections show a distinct decrease of andradite at the expense of grossular ($\text{Alm}_{6.7-7.9}\text{Prp}_{0.3-0.6}\text{Sps}_{1.5-2.0}\text{Uv}_{0-0.3}\text{Gr}_{28.6-32}\text{Adr}_{57.6-61.1}$). As also observed in sample M-25, garnet from YKK-1a contains elevated TiO_2 contents of 2.3 wt-% (core) to 3.1 wt-% (rim). Green clinopyroxene is virtually unzoned aegirine-rich augite and aegirine-augite (classification after Morimoto et al., 1988) showing slightly variable compositions ($\text{Q}_{75.7-82.5}\text{Aeg}_{13.9-18.2}\text{Jd}_{2.4-7.9}$) from grain to grain. Nepheline also yields elevated Si-contents of 8.338–8.413 p.f.u. and X_K -values of 0.151–0.169. Electron microprobe analyses of K-feldspar vary from grain to grain ($\text{Or}_{53.2-76.4}\text{Ab}_{21.8-45.2}\text{An}_{1.1-1.5}\text{Cs}_{0.5-1.1}$) and carbonate is almost pure calcite ($\text{CaCO}_3 > 99.3$ mol-%). Electron microprobe analyses of sample YKK-1a are listed in Tables S1, S3, S5 and S6 of the electronic supplement.

Sample YKK-1c (Fig. 4f) was also part of the central section of the mafic layer and resembles sample YKK-1a. The blurry mafic gneiss yields cm-sized leucocratic patches and does not show any parallel texture (Fig. 6e & f). Microscopic investigations classify the sample as a carbonate-bearing scapolite-garnet-plagioclase-clinopyroxene-nepheline gneiss. Its melanocratic sections prove to be sieve-like intergrowths of green clinopyroxene and nepheline with minor poikiloblastic to granular, pinkish brown garnet. In the felsic lenses elongate, anhedral nepheline crystals are intergrown with large subhedral plagioclase and locally with poikiloblastic scapolite and minor anhedral carbonate. The mineral and grain size distribution of the sample is rather inhomogeneous. Accessories are titanite, apatite and pyrite. Electron microprobe

analyses of garnet show a composition of $\text{Alm}_{11.5-14.9}\text{Prp}_{0.4-0.7}\text{Sps}_{2.1-3.4}\text{Gr}_{57.4-59.9}\text{Adr}_{25.5-27.4}$ and TiO_2 -contents of 1.3–1.7 wt-%, which strongly resembles garnet from the nepheline gneiss M-25. Clinopyroxene is aegirine-rich augite with a composition of $\text{Q}_{80.5-85.8}\text{Aeg}_{13.3-17.3}\text{Jd}_{0.8-2.84}$, which varies from grain to grain. Nepheline yields Si-contents of 8.191–8.456 p.f.u. and X_K -values of 0.117–0.147. Plagioclase shows slight variations in composition from grain to grain ($\text{Ab}_{55.9-58.3}\text{An}_{39.9-41.9}\text{Or}_{1.3-2.3}$). Electron microprobe analyses of scapolite prove a composition halfway between the Ca-endmember meionite and the Na-endmember marialite ($X_{\text{Me}} = 0.499\text{--}0.51$) with Cl-contents of up to 1.67 wt-%, but no fluorine and sulphur. Carbonate is almost pure calcite with $\text{CaCO}_3 > 98.7$ mol-%. Electron microprobe analyses of sample YKK-1c are listed in Tables S1, S3, S4, S6 and S8 of the electronic supplement.

Sample YKK-2d originates from the lower part of the mafic layer and is distinctly more melanocratic than the gneiss from its central section (Fig. 4g). The fine-grained rock is classified as a clinopyroxene-clinoamphibole gneiss, which consists of ultramafic laminae formed by brown Ti-hornblende and clinopyroxene while more felsic, plagioclase-bearing sections are subordinate (Fig. 6g & h). Accessories in this rock are biotite, apatite, titanite and pyrite. Clinopyroxene is augite after the classification of Morimoto et al. (1988) showing a composition of $\text{Wo}_{38.2-41.9}\text{En}_{45.0-47.2}\text{Fs}_{13.1-15.2}$. Remarkably, stoichiometric calculations using the method of Ryburn et al. (1976) yield only low amounts of ferric iron (1–8.3 % of total Fe). Clinoamphibole is Ti-rich pargasite following the classification of Hawthorne et al. (2012) and yields TiO_2 -contents of 1.2–1.5 wt-% and X_{Mg} -values of 0.70–0.74. Biotite shows somewhat variable TiO_2 -contents of 1.9–3.1 wt-% and X_{Mg} -values of 0.70–0.74. Plagioclase is calcic with small variations from grain to grain ($\text{Ab}_{14.7-17.3}\text{An}_{82.7-85.1}$). Electron microprobe analyses of sample YKK-2d are listed in Tables S2, S3, S4 and S7 of the electronic supplement.

4.2. Geothermobarometry

Geothermobarometric investigations were performed using a combination of geothermobarometric methods and equilibrium assemblage diagrams calculated with the Theriak-Domino software (De Capitani and Petrakakis, 2010). The Theriak-Domino software is based on Gibbs free energy minimization of phases and solution models in a thermodynamic database. The database used in this work is mainly tcd65c2, from Holland and Powell (1998), with solution models by Baldwin et al. (2005), White et al. (2007) and Diener et al. (2007). For sample YKK-2d, the clinoamphibole-clinopyroxene gneiss, the database used is tcds62c, from Holland and Powell (2011), with solution models by White et al. (2014a, 2014b) and Green et al. (2016). We chose this database as it supplies an elaborated clinoamphibole model for high-grade mafic rocks (cf. Green et al. 2016), which is not compatible with the tcd655c2 dataset. The databases used in this work can be downloaded at <https://titan.minpet.unibas.ch/minpet/theriak/theruser.html>. For the activity of water, the standard state is the pure phase at P and T and thus is a measure of the “effective concentration” in a mixture.

For rocks with H_2O -bearing phases (i.e., the quartz-garnet gneiss), using these two independent methods not only determines the metamorphic PT-conditions, but also allows estimating the water activity during metamorphism. In granulite facies terrains, the water activity is distinctly reduced as otherwise the rock would melt and form migmatites (cf. Bader et al., 2014 and citations within).

4.2.1. Quartz-garnet gneiss

In sample ALT-03, the biotite-garnet-orthopyroxene gneiss (Fig. 5a & b), the garnet-orthopyroxene-plagioclase quartz geothermobarometer of Lal (1993) yields granulite facies conditions of 758 °C at 7.3 kbar for the garnet analysis with the highest X_{Mg} -value from the core section of the garnet. Temperatures are well in accord with the Ti-in biotite geothermometer of Henry et al. (2005), which yields 766–779 °C. For the garnet rim section, the geothermobarometer of Lal (1993) points to PT-conditions of 725 °C at 6.1 kbar, which highlight a part of the retrograde

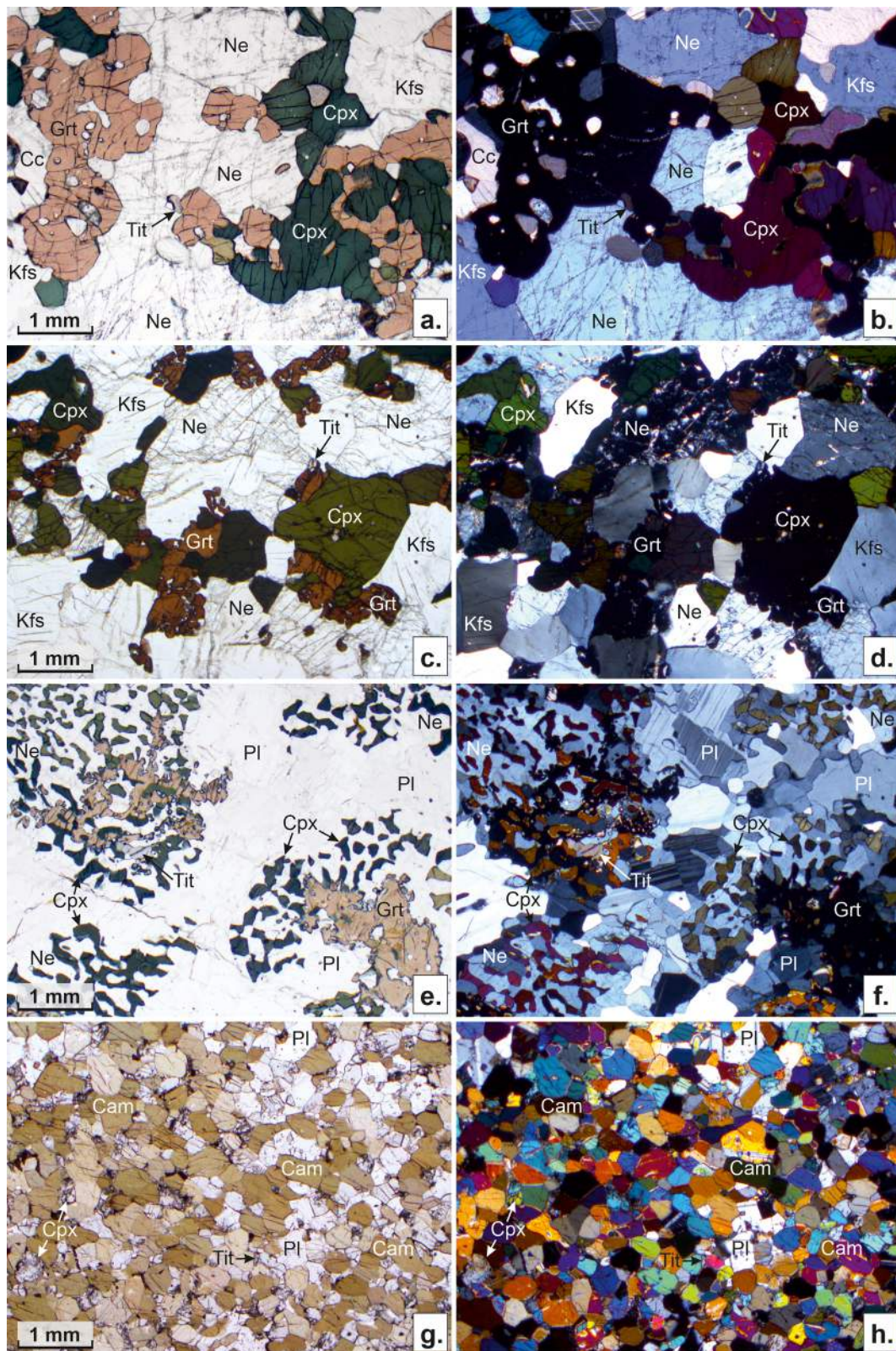


Fig. 6. Microphotographs of nepheline gneiss and clinopyroxene-clinoamphibole gneiss (parallel polarizers on the left side, crossed polarizers on the right side). a. and b.) sample M-25 yields granoblastic brown Grt, dark green, aegirine-rich Cpx, Ne, Kfs, Cc and accessory Tit. c. and d.) sample YKK-1a has the same mineral assemblage as sample M25 with Grt showing dark brown rim sections. e. and f.) sample YKK-1c displays sieve-like intergrowths of green Cpx and Pl surrounding irregular Grt grains and Ne. g. and h.) sample YKK-2d presents a granoblastic fabric made up of brown Ti-rich Cam, Pl and accessory Tit.

PT-path of the rock (Fig. 7a).

Equilibrium phase diagram calculations with the Domino program are strongly dependent on the water activity. Due to the presence of the hydrate mineral biotite in sample ALT-03, water has to be present in the rock. At strongly reduced water activity, the stability field of the observed mineral assemblage is found at rather low temperatures whereas high water activity leads to its reduction and finally to its complete disappearance. Furthermore, high water activity strongly enlarges the field of anatexis in the rock. For this reason, calculations with the Domino program in the TiCaNaKFMASH system were performed for the garnet core section of sample ALT-03 with H₂O in excess and for variable water activities ($a_{\text{H}_2\text{O}}$) ranging from 0.1 to 1. From these calculations, which are shown in detail and commented in the electronic supplement (Electronic supplement - Phase diagram calculations at variable $a_{\text{H}_2\text{O}}$), it becomes evident that the best fit between the Domino calculations and the geothermobarometry is obtained $a_{\text{H}_2\text{O}} = 0.4$ with garnet isopleths intersecting at 743 °C and 6.9 kbar (Fig. 7a). Another method to estimate the water activity in the sample is given by the Theriak-Domino program, which calculates the modal mineral amount of the sample at the intersection point of the garnet isopleths at different $a_{\text{H}_2\text{O}}$ -values. For sample ALT-03, the best fit between the calculated modal amount of minerals and the modal amount determined by point-counting of the thin section is given at $a_{\text{H}_2\text{O}} = 0.2$, which is slightly lower than the estimate using the geothermobarometry data.

Sample BPD-02, the sillimanite-bearing biotite-garnet gneiss (Fig. 5c & d), was investigated thermobarometrically using the garnet composition of the rim section with the highest X_{Mg} . The garnet-biotite geothermometer of Holdaway (2000) in combination with the GASP geobarometer of Koziol and Newton (1988) calculate 792 °C at 7.6 kbar. As garnet in sample BPD-02 is virtually unzoned, calculation using other garnet analyses yields almost identical results. Temperatures of 819–828 °C are calculated with the Ti-in-biotite geothermometer of Henry et al. (2005) reproducing the results of the garnet-biotite thermometry within the error of the methods. Calculations with the Theriak-Domino program in an analogous manner as described for sample ALT-03 indicates the closest fit of the phase diagram with the geothermobarometry at a water activity of 0.34 with garnet isopleths intersecting at 789 °C and 8.4 kbar (Fig. 7b). The best fit between the modal mineral amount calculated at the garnet intersections by the Theriak-Domino program and the modal mineral amount determined by point-counting is at $a_{\text{H}_2\text{O}} = 0.4$.

In biotite-garnet gneiss sample K-01 (Fig. 5e & f), a combination of the garnet-biotite geothermometer of Holdaway (2000) with the garnet-biotite-plagioclase-quartz geobarometer of Wu et al. (2004; Fe-calibration) calculates PT-conditions of 756 °C at 7.4 kbar using a garnet analysis from the rim section. Despite of the absence of a Ti-bearing oxide phase in this sample, the Ti-in-biotite geothermometer of Henry et al. (2005) supplies very similar temperatures of 758–764 °C. Phase diagram calculations using the same approach as in the two foregoing samples yield the closest fit between the Theriak-Domino program and the geothermobarometry at a water activity of 0.4 (Fig. 7c). The best fit of the modal mineral amount calculated at the garnet isopleth intersections by the Theriak-Domino program and the one determined by point-counting is at $a_{\text{H}_2\text{O}} = 0.5$ and thus quite close to the water activity derived using the geothermobarometric estimates.

4.2.2. Garnet-clinopyroxene-nepheline gneiss

Thermobarometric investigations of these unusual rocks are strongly aggravated by their exotic chemical composition, by the lack of thermodynamic data and mixing models for some of the minerals as well as by the elevated oxygen fugacity of the nepheline gneiss, which is mirrored by the high andradite and aegirine components in garnet and clinopyroxene. Despite of these complications, a general estimate of their metamorphic conditions is possible.

The carbonate-garnet-K-feldspar-clinopyroxene-nepheline gneiss M-25 (Fig. 6a & b) shows a tight intergrowth of garnet and

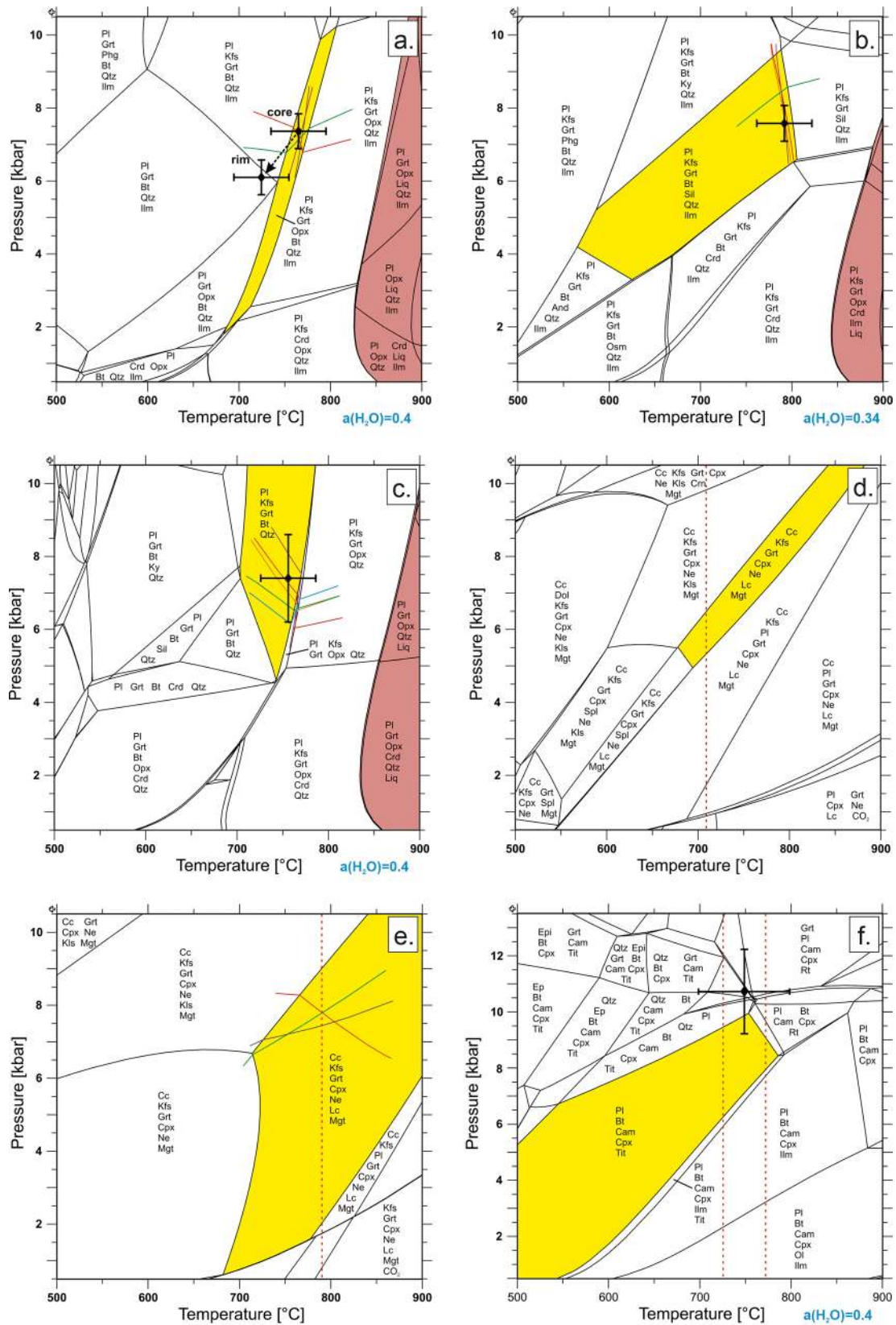
clinopyroxene, which should permit the application of the garnet-clinopyroxene geothermometer. However, calculations using various calibrations of this geothermometer yield widely variable results, which is probably due to the high concentrations of ferric iron in both garnet and clinopyroxene. Ferric iron, however, is not considered by any of the available calibrations. The only geothermobarometric method, which could be applied to this sample, is the nepheline-K-feldspar thermometry of Powell & Powell (1977). To avoid effects of unmixing or inhomogeneity, both minerals were mapped with an enlarged electron microprobe beam of 200 µm and the average compositions were used for the calculations, which results in temperatures of 709 °C. Phase equilibrium calculations with the Theriak-Domino program highlight a stability field for the assemblage calcite - K-feldspar - garnet - clinopyroxene - nepheline - leucite - magnetite at temperatures > 680 °C and pressures > 5 kbar (Fig. 7d). The presence of leucite in the calculated assemblage is due to the occurrence of elevated amounts of K and Si in nepheline (Deer et al. 2004). The garnet isopleths for almandine, grossular and andradite do not have a common intersection. The intersection of the K_D -value of the nepheline-K-feldspar thermometry (dotted red line) with the stability field of the observed mineral assemblage in Fig. 7d, however, points to high-grade metamorphic PT-conditions similar to the neighbouring host rocks (taking into account an error in excess of ± 50 °C for the nepheline-K-feldspar geothermometer; cf. Powell & Powell, 1977).

Sample YKK-1a, a carbonate-bearing garnet-K-feldspar-clinopyroxene-nepheline gneiss (Fig. 6c & d), displays the same mineral assemblage as sample M-25 and permits the application of the same type of geothermobarometry. Similar to sample M-25, garnet-clinopyroxene thermometry yields highly variable results. The nepheline-K-feldspar thermometry of Powell & Powell (1977) calculates temperatures of 790 °C for the integrated nepheline and K-feldspar analyses. Equilibrium phase diagram calculations with the Theriak-Domino program reveal a wide stability field for the assemblage calcite-K-feldspar-garnet-clinopyroxene-nepheline-leucite-magnetite at high temperatures (Fig. 7e). Remarkably, the intersections of the garnet isopleths (Alm, Grs & Adr) plot in a PT-range of 784–812 °C at 7.8–8.4 kbar, which is close to the estimates of the quartz-garnet gneiss from the central part of the Mogok Metamorphic Belt (Fig. 7a-c). There is no intersection for the garnet isopleths of the dark brown garnet rim.

Thermobarometry of sample YKK-1c, a carbonate-bearing scapolite-garnet-plagioclase-clinopyroxene-nepheline gneiss (Fig. 6e & f), does not yield reasonable results as the composition of this K-feldspar-free rock does not permit the use of garnet-clinopyroxene and nepheline-K-feldspar thermometry. Furthermore, the plagioclase-scapolite geothermometer of Goldsmith and Newton (1977) is restricted to Na-poor scapolite and calcic plagioclase. Equilibrium phase diagram calculations using Theriak-Domino do not show a stability field of scapolite, possibly due to the lack of an appropriate solid solution model for scapolite in the tcd55c2 dataset. Therefore, no P-T conditions are reported for this sample.

4.2.3. Clinopyroxene-clinoamphibole gneiss

In the clinopyroxene-clinoamphibole gneiss YKK-2d (Fig. 6g & h), the Ti-in-amphibole geothermometer of Colombi (1988) on the Ti-rich pargasite estimates temperatures of 729–765 °C. This agrees with the amphibole-plagioclase geothermometer of Holland & Blundy (1994), which calculates 774–784 °C. Due to the lack of critical mineral assemblages, a pressure estimate is delicate. A combination of the Ti-in-Hbl geothermometer of Colombi (1988) with the amphibole-plagioclase P_1 -geobarometer of Bhadra and Bhattacharya (2007) using the average composition of all clinoamphibole and plagioclase analyses yields 10.7 kbar at 746 °C. However, due to the absence of quartz in the rock, this pressure estimate represents a maximum value. Equilibrium phase diagram calculations with the Theriak-Domino program and the tcds62c dataset, which supplies a clinoamphibole model for high-grade mafic rocks of Green et al. (2016),



(caption on next page)

Fig. 7. Equilibrium phase diagrams of quartz- and nepheline and clinopyroxene-clinoamphibole gneiss; stability fields of the observed mineral assemblage are shown in yellow and fields of anatexis in reddish-brown, error bars indicate the PT-estimates of the geothermobarometry (see text), bulk values in ions. a.) Bt-Grt-Opx gneiss ALT-03 (bulk = Si(4.525) Ti(0.021) Al(1.137) Fe(0.507) Mg(0.173) Ca(0.167) K(0.217) Na(0.438) H(50) O(36.972)) with isopleths of Alm (red), Grs (green), Prp (violet) and X_{Mg} of Bt (brown) for the peak metamorphic conditions (core); second error bars highlight the retrograde PT-evolution based on the rim composition of the garnet. b.) Sil-Bt-Grt gneiss BPD-02 (bulk = Si(4.339) Al(1.413) Ti(0.031) Fe(0.363) Mn(0.014) Mg(0.245) Ca(0.078) K(0.506) Na(0.363) H(50) O(36.98)) with isopleths of Alm (red), Grs (green), Prp (violet) and Sps (orange); c.) Bt-Grt gneiss K-01 (bulk = Si(4.138) Al(1.336) Fe(0.810) Mg(0.500) Mn(0.026) Ca(0.185) K(0.131) Na(0.161) H(50) O(36.963)) with isopleths of Alm (red), Grs (green), Prp (violet), Sps (orange) and An-content in Pl (blue); d.) Ne gneiss M–25 (bulk = Si(3.252) Al(1.913) Fe(0.341) Mg(0.149) Ca(0.891) Na(1.223) K(0.360) C(0.167) O(12)) with result of the Ne-Kfs thermometry (dotted red line); e.) Ne gneiss YKK-1a (bulk = Si(3.409) Al(1.656) Fe(0.674) Mg(0.068) Ca(0.898) Na(1.147) K(0.343) C(0.037) O(12)) with isopleths of Alm (red), Grs (green), Adr (violet) and result of Ne-Kfs thermometry (red dotted line); f.) Cam-Cpx gneiss YKK-2d (bulk = Si(3.360) Ti(0.082) Al(1.246) Fe(0.590) Mg(1.309) Ca(1.122) K(0.095) Na(0.280) H(50) O(37)) with range of the Ti-in-Hbl thermometry (red dotted lines). Note that the error bar only displays maximum pressures for the rock.

shows a wide stability field for the observed mineral assemblage in the sample (Fig. 7f). An intersection of the Ti-in Hbl barometry with this stability field indicates PT-conditions of 730–765 °C at 6.2–9.5 kbar at $a_{H_2O} = 0.4$, which is in accord with the results from the other samples.

4.3. Whole-rock geochemistry of carbonate-bearing clinopyroxene-nepheline gneiss and clinopyroxene-clinoamphibole gneiss

The carbonate-bearing clinopyroxene-nepheline gneiss and clinopyroxene-clinoamphibole gneiss are high-K calc-alkaline (YKK-1c, YKK-2d) and shoshonitic (M–25, YKK-1a) rocks (cf. Fig. 8a). The nepheline bearing rocks are characterized by variable, but low to moderate SiO_2 contents (39.1 to 50.4 wt-%), relatively low MgO contents (0.62 to 1.39 wt-%), and high $Na_2O + K_2O$ contents (7.57 to 11.1 wt-%) and correspond chemically to foidite, phonotephrite, or tephriphonolite (Fig. 8b). The low contents of the compatible elements Ni and Cr in combination with the low MgO contents indicate that these rocks have experienced significant fractionation. These rocks have high CaO contents that range from 6.96 wt-% to 19.6 wt-% (Table S9). Alkaline magmatic rocks with these chemical signatures may be obtained by fractionation of clinopyroxene, which reduces the contents of Mg, Ni, and Cr and allows for an increase of SiO_2 (Table S9). The high CaO contents may represent a source signature, as for leucitites and foidites (e.g., Lustrino et al., 2019; Prelević et al., 2015) or reflect assimilation of carbonate wall-rocks. The clinopyroxene-clinoamphibole gneiss has high MgO (12.5 wt-%) and relatively low contents of $Na_2O + K_2O$ (2.43 wt%) and may originally have been a microbasalt. This sample has high contents of the compatible elements Co, Ni, and Cr (Table S9) and, therefore, did not experience significant fractionation. Calculations of the CIPW normative mineralogy (total Fe = Fe^{2+}) show that all these rocks are nepheline-normative and that samples YKK-1a and M–25 also contain leucite.

The MORB-normalized spidergrams of the nepheline-bearing metadykes (YKK-1a, YKK-1c and M–25) from Myanmar are strongly enriched in Cs, Rb, Ba, Th and U, show positive anomalies in K and Pb and variably negative anomalies for Ti, Nb and possibly Ta (Fig. 9a). Whereas the negative anomalies (Ta, Nb, Ti) are hallmark geochemical fingerprints for magmatic rocks that formed in a subduction setting, the positive anomalies in K and Pb are typical for melts derived from the lithospheric mantle that had been modified by fluids or melts released from subducted continent-derived sedimentary rocks (Lee et al., 2016; Lustrino et al., 2019; Campbell et al., 2014). Although the clinopyroxene-clinoamphibole gneiss YKK-2d has a broadly similar pattern as the other rocks and also has negative Nb and Ti anomalies, it does not have such a strong enrichment of alkali and alkaline earth metal elements (Fig. 9a).

The Pb isotopic compositions of all metamorphosed dykes fall in a relatively narrow range with $^{206}Pb/^{204}Pb$ values of 18.32 to 18.97 and very high $^{207}Pb/^{204}Pb$ values of 15.71 to 15.76 (Fig. 10a and Table S10, recalculated data). Such high $^{207}Pb/^{204}Pb$ values imply derivation of Pb from very old, i.e., Paleoproterozoic or Archean, continental crust. The relatively high $^{208}Pb/^{204}Pb$ values of 38.47 to 39.16 at a given $^{206}Pb/^{204}Pb$ (Fig. 10b) make these samples fall above typical upper crustal and orogenic Pb growth curves and therefore indicate that this

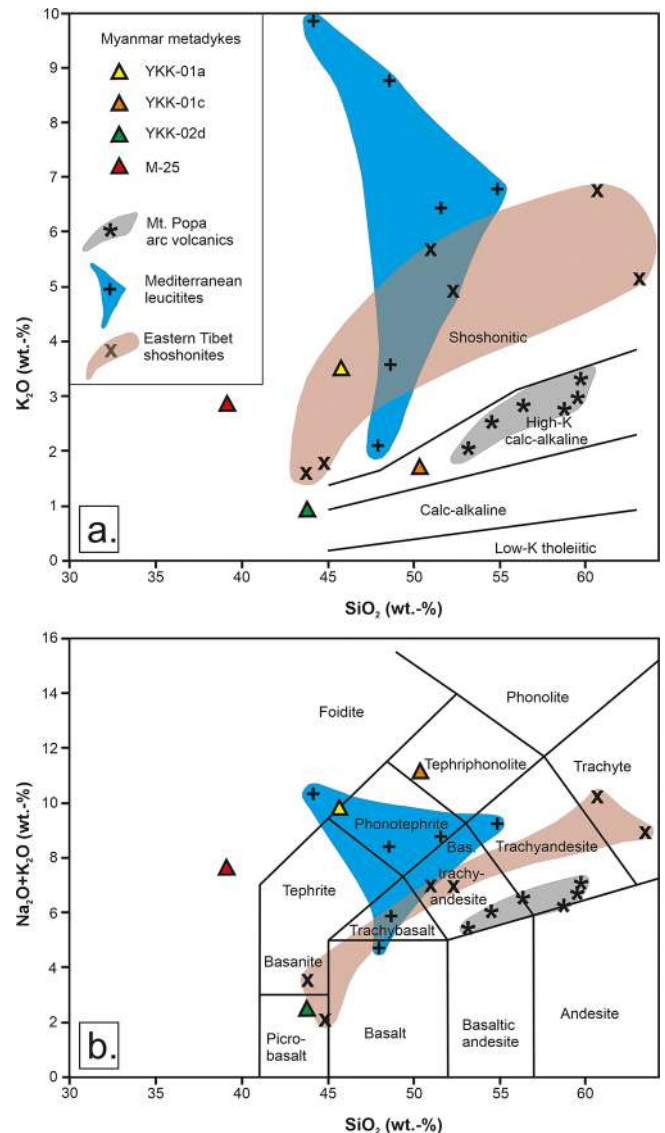


Fig. 8. (a) K_2O vs SiO_2 -diagram with series boundaries after Rickwood (1989) and b.) Total alkali vs silica diagram after Le Bas et al. (1986). Reference fields for mantle-derived rocks from Lee et al. (2016), Lustrino et al. (2019) and Campbell et al. (2013).

crustal material also includes contribution of material that had high Th/Pb ratios for a geologically extended period. There are two processes that result in high Th/Pb ratios, i.e., high-grade metamorphism (Zartman and Doe, 1981) and intense chemical weathering (e.g., Franz et al., 2013; Romer et al. 2014). Both processes result in the preferential loss of Pb and U relative to Th, which retards the increase in $^{206}Pb/^{204}Pb$ with time relative to the increase in $^{208}Pb/^{204}Pb$ (Zartman and Doe, 1981).

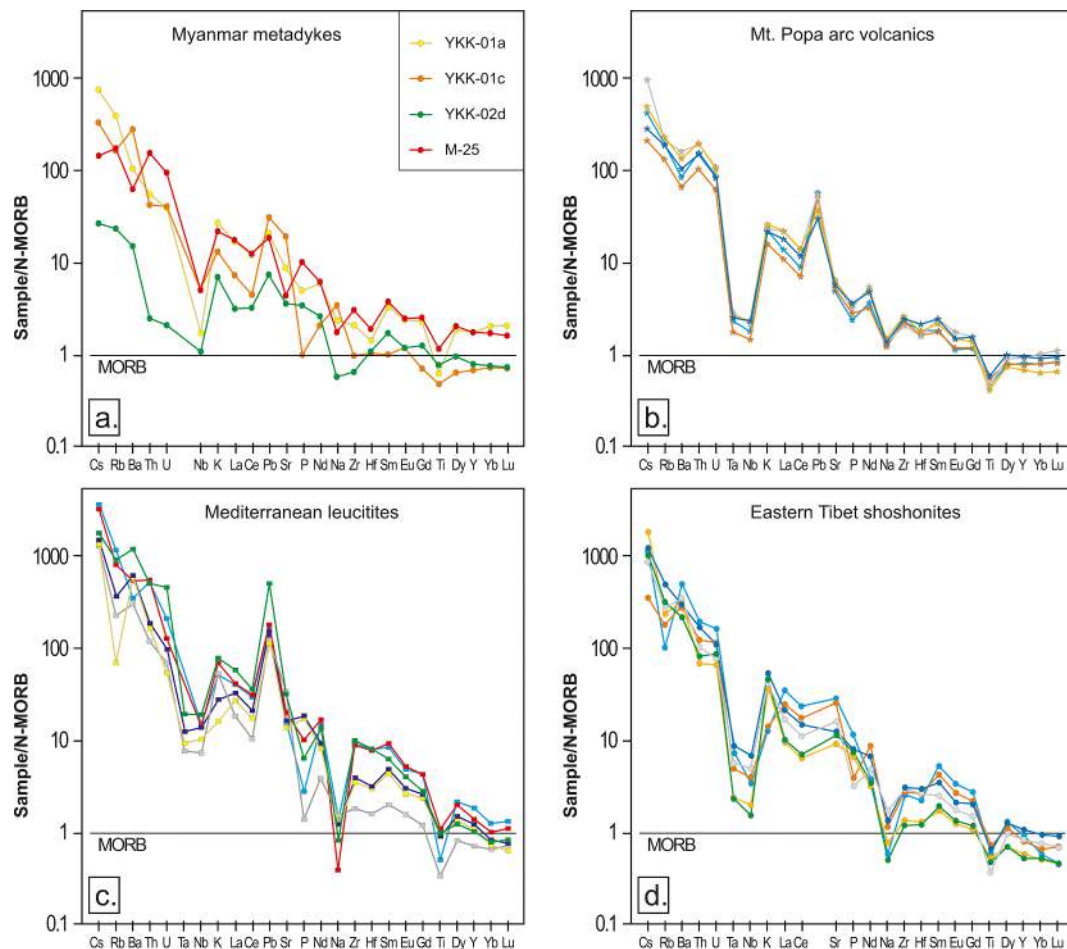


Fig. 9. MORB-normalized spidergrams for a.) Myanmar metadykes (this study); b.) Mid-Miocene calc-alkaline arc volcanites from Mt. Popa, Myanmar (Lee et al., 2016); c.) leucitites from the Eastern Mediterranean and Iran (cf. Lustrino et al., 2019) d.) Subduction-related shoshonites from Eastern Tibet (Campbell et al., 2013). N-MORB normalization values from Pearce and Parkinson (1993).

In the $^{143}\text{Nd}/^{144}\text{Nd}$ vs $^{87}\text{Sr}/^{86}\text{Sr}$ diagram, the metamorphosed dykes fall in a cluster between the fields for the depleted mantle (MORB) and continental crust (Fig. 11 and Table S10), which typically defines sub-horizontal fields reflecting the relatively narrow range of $^{147}\text{Sm}/^{144}\text{Nd}$ ratios and the broad range in $^{87}\text{Sr}/^{86}\text{Sr}$ ratios of crustal rocks. The lower the initial $^{143}\text{Nd}/^{144}\text{Nd}$ ratio of the crustal field, the older the average age of the crustal source. Typical Neoproterozoic and Archean continental crust has ϵNd_{30} values around -18 and -30 , which indicates that the Nd isotopic compositions of the mafic metadykes reflect 60 to 70 % contribution of old crustal Nd from the subducted material (Fig. 11 and Table S10).

5. Discussion

Metamorphosed mafic dykes occur throughout the Mogok Stone Tract and typically occur in close spatial relation with marble-hosted spinel and ruby gemstone deposits. It is a priori not clear whether this spatial relation is coincidental (better exposure in the mining areas also exposes more dykes) or whether the dykes contributed to conditions that favoured formation of gemstone deposits during later high-grade metamorphism. The close spatial relation between dykes and gemstone deposits allows to use PT conditions of the dykes to constrain the PT conditions of gemstone deposits, which have restricted mineral assemblages that do not allow for PT determination. In the following, we discuss the origin of the mafic rocks, the relation of the mafic dykes with their carbonate host and their common metamorphism.

The chemistry of the mafic dykes (now nepheline gneiss) classifies

their protoliths as high-K calc-alkaline and shoshonitic magmatites (Fig. 8) that are derived from the partial melting of lithospheric mantle. Typical for such mantle-derived rocks are high contents of K_2O and incompatible trace elements (Figs. 8 and 9) reflecting a two-stage process in the subduction zone, i.e., depletion of the mantle by partial melting followed by metasomatism of the depleted mantle by fluids and melts derived from subducted sedimentary or crustal material. Later changes in the slab geometry resulted in extension with adiabatic melting of metasomatized domains (e.g., Lustrino et al., 2019; Prelević et al., 2015). Such melts have high Mg, Ni, and Cr contents and high contents of incompatible elements. Fractional crystallization reduces the contents of the compatible elements Mg, Ni, and Cr in the melt. All samples of nepheline gneiss have low X_{Mg} -values and low Ni and Cr contents, indicating that these melts fractionated before emplacement. In contrast, the clinopyroxene-clinoamphibole gneiss has a higher X_{Mg} -value and a different trace element pattern, possibly reflecting both a different degree of fractionation and a different magma source.

This process explains why mantle-derived mafic rocks have trace element patterns and Sr-Nd-Pb isotopic compositions typical for crustal rocks. Typically, these rocks show an enrichment in Cs, Rb, K, Ba, Pb and the light REE and a depletion in Ti, Nb and Ta in MORB-normalized spidergrams (Fig. 9). This two-stage process explains why comparable rocks from different regions such as the trachyandesites from Mt. Popa, shoshonites from eastern Tibet as well as Mediterranean leucitites have similar trace element patterns (Fig. 9a-d). The Sr, Nd and Pb isotopic composition of these rocks also reflects their crustal source, but may show regional differences depending on the age of the source. For

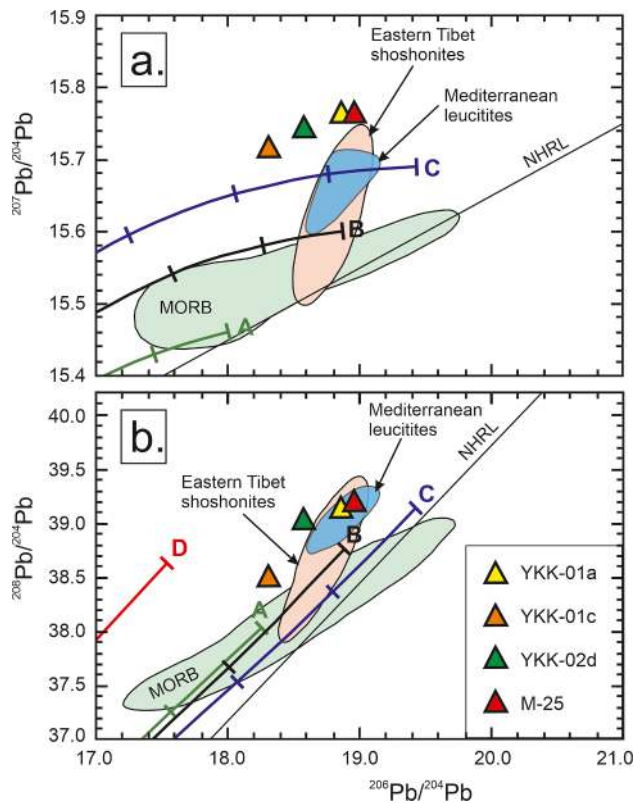


Fig. 10. (a.) Plot of $^{207}\text{Pb}/^{204}\text{Pb}$ against $^{206}\text{Pb}/^{204}\text{Pb}$ and b.) Plot of $^{208}\text{Pb}/^{204}\text{Pb}$ against $^{206}\text{Pb}/^{204}\text{Pb}$. Data for MORB, Eastern Tibet shoshonites, and NHRL (Northern Hemisphere Reference Line) from Campbell et al. (2014), Mediterranean leucitites after Lustrino et al. (2019). Lead-isotope evolution curves according to Zartman & Doe (1981): (A) mantle, (B) orogen, (C) upper crust, and (D) lower crust. Tick marks along each curve indicate 0.4 Ga increments.

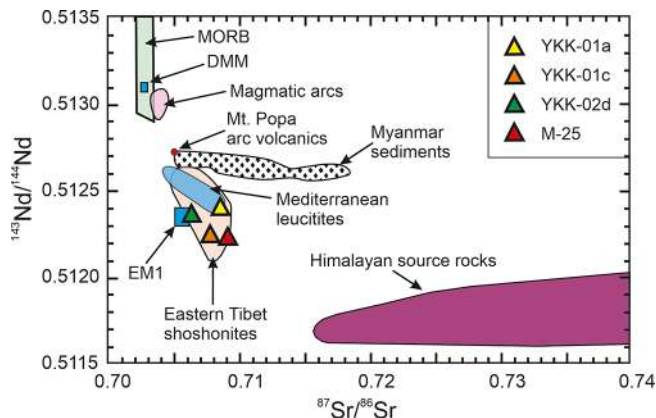


Fig. 11. Plot of $^{143}\text{Nd}/^{144}\text{Nd}$ against $^{87}\text{Sr}/^{86}\text{Sr}$ with the metadykes from Myanmar, MORB and Eastern Tibet shoshonites (Campbell et al. 2014), Mediterranean leucitites (Lustrino et al., 2019), magmatic arc volcanics from Marianas, New Britain, Aleutians, South Sandwich and Lesser Antilles (Arculus and Powell, 1986), arc volcanics from Mt. Popa (red spot; Lee et al., 2016) and Myanmar sediments (Licht et al., 2013). Isotope data of enriched mantle (EM1) and depleted mantle (DMM) from Faure (2001; page 314). Himalayan source rocks for subduction from Ahmad et al. (2000), Miller et al. (2001) and Richards et al. (2005).

instance, the investigated mantle-derived mafic dykes have lower ϵNd_{30} values than regional or local magmatic arc rocks that were extracted from the mantle (e.g., Mt Popa arc volcanics, Fig. 11). The subduction of

local sedimentary rocks also would produce a metasomatized mantle with too high ϵNd_{30} values (Fig. 11). Instead, the mafic dykes compositionally resemble to shoshonitic rocks that are derived from a mantle metasomatized by Paleoproterozoic or Archean crust (or sediments derived from such a crust; Fig. 11). If the crustal component is derived from Paleoproterozoic or Archean crust, mass balance indicates that the 60 to 70 % of the Nd budget of the mafic dykes is derived from the subducted material (Fig. 11 and Table S10). The Pb isotopic composition reflects an old crustal source for the subducted sediments. The old crust, however, does not have to be the direct source. Instead, the recycling of old continental crust during collisional processes and erosion does not erase the Pb isotopic signature of the crust. The Pb isotopic compositions of sediments from the Himalayan orogen represent Pb from such a recycled ancient crust (see Richards et al., 2005 and references within). Sediments from a similar source may have metasomatized the lithospheric mantle sampled by the investigated dykes.

The metadykes have elevated to high Ca and Sr contents, which could reflect a chemical fingerprint of the mantle source or could be the result of interaction between the mafic melts and the hosting calcisilicate rock and marble. Such an interaction would only increase Ca and Sr contents of the melt, as the contents of most other trace elements are low in carbonates, and shift the Sr isotopic composition of the melt toward the composition of the carbonates. Furthermore, it could decrease the SiO_2 contents of these alkaline magmatic rocks (e.g., Conte et al., 2009; Elitok, 2019). There are three lines of evidence indicating that interaction between the alkaline melts and the carbonates was limited: (i) Reaction rims between mafic rocks and carbonates are absent or thin; (ii) Addition of carbonates would increase both Ca and Sr contents together, but the sample with the lowest Ca content has the highest Sr content and there is a general tendency for samples with high Ca contents to have systematically lower Sr contents; (iii) Interaction with the graphite- and pyrite-rich carbonates should reduce the oxygen fugacity of the alkaline melts, which is not the case. The mafic rocks still have very high oxygen fugacity, in part contributing to the particular mineralogical composition of the metamorphic rocks.

The observed mineral parageneses as well as the recorded PT-conditions of the investigated gneiss samples from the Central and Western Part of the Mogok Stone Tract confirm granulite facies conditions. Geothermobarometry reveals temperatures between $709 (\pm 50)^\circ\text{C}$ (sample M-25, nepheline-K-feldspar geothermometer) and $828 (\pm 25)^\circ\text{C}$ (sample BPD-02, Ti-in biotite geothermometer) as well as pressures between $7.3 (\pm 0.5)$ kbar (sample ALT-03; Grt-Opx-Pl geobarometer) and $10.7 (\pm 1.5)$ kbar (YKK-2d, Cam-Pl geobarometer). PT-estimates on quartz-garnet gneiss using geothermometers and geobarometers suitable for high-grade metamorphic conditions indicate a PT-range of $756\text{--}792 (\pm 30)^\circ\text{C}$ at $7.3\text{--}7.6 (\pm 0.5\text{--}1.0)$ kbar. These PT-conditions agree with thermobarometric investigations of Thu and Enami (2018) revealing granulite facies conditions of $780\text{--}810^\circ\text{C}$ at 8 kbar in calcisilicate marble from the Western part of the Mogok area.

U-Pb ages of zircon inclusions in ruby and spinel as well as of zircon from host rocks from the Mogok area (Phyo et al., 2020) demonstrate that ruby and spinel deposits in Mogok formed during Oligocene to Early Miocene regional granulite-facies metamorphism related to the Himalayan Orogeny.

Granulite facies metamorphism may occur under fluid absent or fluid present conditions. For the calculation of granulite facies PT-conditions, numerous researchers (e.g. Tajčmanová et al. 2006, Xiang et al. 2012) use a fixed but limited amount of H_2O , which implies the absence of a free fluid at certain metamorphic PT-conditions and therefore dry conditions. The worldwide observation of fluid inclusions in granulite facies rocks (e.g. Touret 1971, Newton et al. 1998, Santosh and Omori 2008, Touret and Huizenga 2012, Bader et al. 2014) renders fluid-absence unlikely. Granulite facies hydrate minerals like biotite and clinopyroxene in the investigated samples and the widespread occurrence of marble in the Mogok belt highlight the presence of H_2O and CO_2 while the occurrence of scapolite in marble and metadykes points to NaCl

contents in the fluid. Therefore, the Theriak-Domino calculations of this study were performed with H₂O in excess but with controlled water activity. The combination of equilibrium phase diagram calculations using the Theriak-Domino program and geothermobarometry applied on quartz-garnet gneiss produces consistent PT-estimates within the error of the methods and reveals water activities of 0.34–0.4 for the investigated samples. The calculated water activities are similar to those calculated with the Theriak-Domino program for felsic and mafic granulites from the Tongbai in east-central China (Bader et al. 2014).

The presence of garnet-nepheline gneiss in association with clinopyroxene-clinoamphibole gneiss within spinel- and ruby-bearing marble and calcisilicate rock is quite remarkable. Nepheline-gneiss and corundum-bearing gneiss have been described from several locations worldwide, e.g. from the Haliburton-Bancroft area of Ontario (USA), where they are assumed to have formed by magmatic interaction of granite with calcisilicate rock and mafic gneiss (Moyd, 1949). Different types of nepheline gneiss also occur in the vicinity of the Darkainle nepheline-syenite complex in Somali, where they formed during metasomatic processes in high-grade, migmatitic host rocks of syenite (Gelatly & Hornung, 1968). In the Ilomba and Ulindi complexes of the North Nyasa Alkaline Province (Malawi), nepheline gneiss was generated by pre- to syntectonic intrusions of nepheline syenite under upper greenschist- to amphibolite facies conditions (Eby et al., 1998). None of these nepheline rocks, however, bears any garnet and none of them experienced granulite facies metamorphic conditions, which makes the Mogok nepheline gneiss unique.

The blastesis of aegirine-rich clinopyroxene, garnet with a high andradite component and magnetite reflects the remarkably high oxygen fugacity of the garnet-nepheline gneiss from Mogok. Such an elevated oxygen fugacity is typical for alkaline arc-related magmatic rocks (Frost & Lindsley, 1992; Müller et al., 2001).

The formation of spinel, ruby and particularly of sapphire in the Mogok area is highly debated, largely as there are several processes that may result in the formation of those minerals and different processes may predominate in different regions. Searle et al. (2020) relate the growth of those gemstones to the thermal and metasomatic interaction between syenite and charnockite intrusions and nearby carbonate or calcisilicate rocks. Because of the polyphase magmatic activity and the polymetamorphic overprint of the rock successions in the Mogok Belt (Searle et al. 2007, 2017), an unequivocal assignment of the gemstone blastesis to a particular event is problematic (Searle et al., 2020). Sutherland et al. (2019) describe metasomatically influenced growth of ruby due to the intrusion of large alkali syenite and ijolite dykes from the deposit Thurein Taung in the Mogok area and link the growth of ruby to magmatism as evident from euhedral nepheline inclusions in ruby from a skarn. This explanation does not apply for the deposit Yadanar Kaday Kadar, as an influence of the metadyke on the formation of spinel and ruby in the deposit can largely be excluded. The metadyke, which has a thickness of about 2 m, is simply too small to impose prominent thermal or geochemical effects on the mighty, about 18 m thick sequence of marble. Furthermore, there is no remarkable, ruby- and spinel-bearing metasomatic alteration zone around the metadyke. Therefore, the growth of spinel and ruby in the Mogok area may be predominantly related to regional metamorphic processes in some deposits and to metasomatic processes in other deposits.

Although we studied the host rocks rather than the gemstone deposits themselves, the *gem* deposits and the surrounding rock formations had the same metamorphic history and, therefore, our results imply that the gemstones developed during granulite facies metamorphism. This inference is supported by inclusions of granulite facies minerals in spinel from Mogok (Phyo et al., 2019) and coincides with the findings for marble-hosted spinel and ruby deposits in East Africa, which formed under granulite facies conditions at ~ 750 °C and 10 kbar (Balmer et al. 2017). In comparison, other marble-hosted spinel and ruby deposits in the Himalayan Mountain Range are reported to have formed at significantly lower PT-conditions than the examined deposits in the Mogok

Stone Tract (Garnier et al., 2008). This would set the ruby and spinel formation in Mogok apart from similar deposits which are related to the collision of the Indian and Asian plate elsewhere.

6. Conclusions

Subduction-related mafic to ultramafic magmas from the lithospheric mantle were emplaced into the carbonates of the Mogok Stone Tract prior to Paleogene high-grade regional metamorphism. There was only limited exchange between mafic magma and the carbonate wall rocks as shown by the absence of metasomatic contact zones and the consistently high oxygen fugacity in the mafic rocks. These mafic dykes and the *gem* deposits are spatially closely related and, therefore, experienced the same conditions of peak metamorphism.

Geothermobarometry and equilibrium phase diagram calculations using the Theriak-Domino program on these metadykes and on garnet-quartz gneiss reveal granulite facies metamorphic conditions for this part of the Mogok Metamorphic Belt. The most precise thermobarometric estimates in quartz-garnet gneiss indicate peak metamorphic PT-conditions ranging from 756 to 792 °C at 7.3–7.6 kbar, which agrees with earlier investigations of the same area (e.g., Thu et al., 2016; Thu and Enami, 2018). The reduced water activity of 0.34–0.4 recorded in the hosting gneiss may reflect dilution by CO₂ from the spinel- and ruby-hosting marble successions. These granulite facies PT-conditions also triggered the formation of spinel and ruby in the Mogok area. Garnier et al. (2008) showed that ruby and spinel in high-grade rocks did not form during peak metamorphic conditions but were generated on the retrograde PT-path under amphibolite facies conditions of 620–670 °C at 2.2–3.3 kbar. In case of the marble-hosted *gem* deposits of the Mogok belt, the presence of paragenetic high-grade metamorphic inclusions in spinel (Phyo et al. 2019) provides strong evidence for their granulite facies formation.

CRedit authorship contribution statement

Myint Myat Phyo: Investigation. **Leander Franz:** Writing – original draft, Supervision. **Rolf L. Romer:** Geochemical and isotope analysis. **Christian de Capitani:** Formal analysis, Supervision. **Walter A. Balmer:** Methodology. **Michael S. Krzemnicki:** Funding acquisition.

Declaration of Competing Interest

The authors declare that they have no known competing financial interests or personal relationships that could have appeared to influence the work reported in this paper.

Data availability

Data will be made available on request.

Acknowledgements

We thank local mining companies and miners for access to their mines and for the donation of fascinating samples. Specifically, we would like to thank Miemie Tin Thut (Silken East Co. Ltd, Bangkok) and Kyaw Swar Htun (AGGL Gem Lab, Yangon, Myanmar) for their generous support in this project. We also thank Ah Ba and Aunty Phyu for their kind encouragement and Sebastian Hänsel, Ko Choo, U Aung Kyaw Htoon and Ko Ja Mu for their help during the field trip to the Mogok area, Myanmar. Special thanks are due to Pascal Tschudin for the perfect preparation of rock sections. We owe thanks to Anja Schleicher, Heike Rothe, Sabine Tonn, and Bettina Hübner (all GFZ) for help with the chemical and isotopic analyses. We gratefully acknowledge the helpful and inspiring reviews of Kurt Bucher (Freiburg) and an anonymous reviewer. This study was financed by a grant from Kanton Basel (Stipendienkommission für Nachwuchskräfte aus Entwicklungsländern), by

a research grant from FAG (Freiwillige Akademische Gesellschaft Basel) and by the Swiss Gemmological Institute SSEF (Basel).

Appendix A. Supplementary data

Supplementary data to this article can be found online at <https://doi.org/10.1016/j.jaesx.2022.100132>.

References

- Ahmad, T., Harris, N., Bickle, M., Chapman, H., Bunbury, J., Prince, C., 2000. Isotopic constraints on the structural relationships between the lesser Himalayan series and the high Himalayan crystalline series, Garhwal Himalaya. *Geol. Soc. Am. Bull.* 112, 467–477.
- Arculus, R.J., Powell, R., 1986. Source component mixing in the regions of arc magma generation. *J. Geophys. Res.* 91, 5913–5926.
- Bader, T., Franz, L., De Capitani, C., Zhang, L., 2014. The effect of water activity on calculated phase equilibria and garnet isopleth thermobarometry of granulites, with particular reference to Tongbai (east-central China). *Eur. J. Mineral.* 26, 5–23.
- Baldwin, J.A., Powell, R., Brown, M., Monares, R., Fuck, R.A., 2005. Modelling of mineral equilibria in ultrahigh-temperature metamorphic rocks from the Anapolis-Itaucu Complex, central Brazil. *J. Metam. Geol.* 23, 511–531.
- Balmer, W.A., Hauenberger, C.A., Fritz, H., Sutthirath, C., 2017. Marble-hosted ruby deposits of the Morogoro Region, Tanzania. *J. Afr. Earth Sci.* 134, 626–643.
- Barley, M.E., Pickard, A.L., Zaw, K., Rak, P., Doyle, M.G., 2003. Jurassic to Miocene magmatism and metamorphism in the Mogok metamorphic belt and the India-Eurasia collision in Myanmar. *Tectonics* 22, 1–11.
- Bender, F., 1983. *Geology of Burma*. Borntraeger, 293 pp.
- Bertrand, G., Rangin, C., Maluski, H., Han, T.A., Thein, M., Myint, O., 1999. Cenozoic metamorphism along the Shan scarp (Myanmar): evidences for ductile shear along the Sagaing fault or the northward migration of the eastern Himalayan syntaxis? *Geophys. Res. Lett.* 26, 915–918.
- Bertrand, G., Rangin, C., Maluski, H., Bellon, H., 2001. Diachronous cooling along the Mogok Metamorphic Belt (Shan Scarp, Myanmar): the trace of the northward migration of India-Indochina oblique convergence since the Oligocene. *J. Asian Earth Sci.* 19, 649–659.
- Bhadra, S., Bhattacharya, A., 2007. The barometer tremolite + tschermakite + 2 albite = 2 pargasite + 8 quartz: Constraints from experimental data at unit silica activity, with application to garnet-free natural assemblages. *Am. Mineral.* 92, 491–502.
- Brown, B., Judd, J.W., 1896. The rubies of Burma and associated minerals: their mode of occurrence, origin, and metamorphoses. A contribution to the history of corundum. *Philos. Trans. Royal Soc. Lond. Ser. A* 187, 151–228.
- Campbell, I.H., Aleksandr, S., Stepanov, A.S., Liang, H.-Y., Allen, C.M., Norman, M.D., 2013. The origin of shoshonites: new insights from the Tertiary high-potassium intrusions of eastern Tibet. *Contrib. Miner. Petrol.* 167, 983–1005.
- Campbell, I.H., Stepanov, A.S., Liang, H.Y., Allen, C.M., Norman, M.D., Zhang, Y.Q., Xie, Y.W., 2014. The origin of shoshonites: New insights from the Tertiary high-potassium intrusions of eastern Tibet. *Contrib. Miner. Petrol.* 167, 1–22.
- Chhibber, H.L., 1934. *The Geology of Burma*. Macmillan and Co., St.Martin's Street, London, 538 pp.
- Colombi, A., 1988. Métamorphisme et géochimie des roches mafiques des Alpes ouest-centrales (Géoprofil Viège-Domodossola-Locarno). PhD thesis, *Mém. Geol. Lausanne* 4, 195 pp.
- Conte, A.M., Dolfi, D., Gaeta, M., Misiti, V., Mollo, S., Perinelli, C., 2009. Experimental constraints on evolution of leucite-basanite magma at 1 and 10–4 GPa: implications for parental compositions of Roman high-potassium magmas. *Eur. J. Mineral.* 21, 763–782.
- De Capitani, C., Petrakakis, K., 2010. The computation of equilibrium assemblage diagrams with Theriak/Domino software. *Am. Mineral.* 95, 1006–1016.
- Deer, W.A., Howie, R.A., Zussman, M.A., 1992. An introduction to the rock forming minerals. Longman, London, 720 pp.
- Deer, W.A., Howie, R.A., Zussman, M.A., 2004. *Rock forming minerals* Vol. 4B, Framework silicates: silica minerals, feldspatoids, and the zeolites. Geological Society of London, 982 pp.
- Dewey, J.F., Cande, S., Pitman, W.C., 1989. Tectonic evolution of the India/Eurasia Collision Zone. *Ecolgae Geol. Helv.* 82, 717–734.
- Diener, J.F.A., Powell, R., White, R.W., Holland, T.J.B., 2007. A new thermodynamic model for clino- and orthoamphiboles in Na₂O-CaO-FeO-MgO-Al₂O₃-SiO₂-H₂O-O. *J. Metam. Geol.* 25, 631–656.
- Eby, N., Woolley, A.R., Din, V., Platt, G., 1998. Geochemistry and petrogenesis of nepheline syenites: Kaungu-Chipala, loba, and Ulindi nepheline syenites intrusions, North Nyasa alkaline Province, Malawi. *J. Petrol.* 39, 1405–1424.
- Elitok, Ö., 2019. Geology and petrology of the potassic and ultrapotassic rocks from the northern part of Senirkent (Isparta-SW Turkey): evidence of magma-carbonate wall-rock interactions. *Arab. J. Geosci.* 12, 289–312.
- Faure, G., 2001. *Alkaline Igneous Rocks on the Continents*. In: Springer, H. (Ed.), *Origin of Igneous Rocks*. Springer Verlag Berlin, Heidelberg, pp. 281–350.
- Fermor, L.L., 1930. General report for the Geological Survey of India. Records of the Geological Survey, India, p. 130.
- Franz, L., Harlow, D.E., 1998. High grade K-feldspar veining in granulites from the Ivrea-Verbano Zone, Northern Italy: fluid flow in the lower crust and implications for granulite facies genesis. *J. Geol.* 106, 455–472.
- Franz, L., Romer, R.L., De Capitani, C., 2013. Protoliths and phase petrology of whiteschists. *Contrib. Miner. Petrol.* 166, 255–274.
- Frost, B.R., Lindsley, D.H., 1992. Equilibria among Fe-Ti oxides, pyroxenes, olivine, and quartz: part II. Application. *Am. Mineralogist* 77, 1004–1020.
- Gardiner, N.J., Robb, L.J., Searle, M.P., 2014. The metallogenic provinces of Myanmar. *Appl. Earth Sci. (Trans. Inst. Min. Metall. B)* 123, 25–38.
- Gardiner, N.J., Searle, M.P., Robb, L.J., Morley, C.K., 2015. Neo-Tethyan magmatism and metallogeny in Myanmar – an Andean analogue? *Journal of Asian Earth Sciences* 106, 197–215. Garnier, V., Ohnenstetter, D., Giuliani, G., Maluski, H., Delouie, E., Trong, T.P., 2005. Age and significance of ruby-bearing marble from the Red River Shear Zone, Northern Vietnam. *Can. Mineral.* 43, 1315–1329.
- Garnier, V., Maluski, H., Ohnenstetter, D., Giuliani, G., Schwarz, D., 2006. Ar-Ar and U-Pb ages of marble-hosted ruby deposits from central and southeast Asia. *Can. J. Earth Sci.* 43, 509–532.
- Garnier, V., Long, P.V., Fallick, A.E., Maluski, H., Lhomme, T., Giuliani, G., 2008. Marble-hosted ruby deposits from Central and Southeast Asia: Towards a new genetic model. *Ore Geol. Rev.* 34, 169–191.
- Gellatly, D.C., Hornung, G., 1968. Metasomatic nepheline-bearing gneisses from Darkainle Somali Republic. *J. Geol.* 76, 678–691.
- Giuliani, G., Fallick, A.E., Garnier, V., France-Lanord, C., Ohnenstetter, D., Schwarz, D., 2005. Oxygen isotope composition as a tracer for the origins of rubies and sapphires. *Geology* 33, 249–252.
- Giuliani, G., Lhomme, T., Dubessy, J., Ohnenstetter, D., Banks, D.A., 2015. Fluid inclusions in ruby from Asian marble deposits: genetic implications. *Eur. J. Mineral.* 27, 393–404.
- Giuliani, G., Fallick, A.E., Boyce, A.J., Pardieu, V., Pham, V.L., 2017. Pink and red spinels in marble: Trace elements, oxygen isotopes, and sources. *Can. Mineral.* 55, 743–761.
- Goldsmith, J.R., Newton, R.C., 1977. Scapolite-plagioclase stability relations at high pressures and temperatures in the system NaAlSi₃O₈-CaAl₂Si₂O₈-CaCO₃-CaSO₄. *Am. Mineral.* 62, 1063–1081.
- Green, E.C.R., White, R.W., Diener, J.F.A., Powell, R., Holland, T.J.B., Palin, R.M., 2016. Activity-composition relations for the calculation of partial melting equilibria in metabasic rocks. *J. Metam. Geol.* 34, 845–869.
- Gübelin, E.J., Koivula, J.I., 1986. *Photoatlas of inclusions in gemstones*. ABC Edition 532 pp.
- Gübelin, E.J., Koivula, J.I., 2005. *Photoatlas of Inclusions in gemstones* Vol. 2, 829 pp.
- Hawthorne, F.C., Oberti, R., Harlow, G.E., Maresch, W.V., Martin, R.F., Schumacher, J. C., Welch, M.D., 2012. Nomenclature of the amphibole supergroup. *Am. Mineral.* 97, 2031–2048.
- Henry, D.J., Guidotti, C.V., Thomson, J., 2005. The Ti-saturation surface for low-to-medium pressure metapelitic biotites: implications for geothermometry and Ti-substitution mechanisms. *Am. Mineral.* 90, 316–328.
- Holdaway, M.J., 2000. Application of new experimental and garnet Margules data to the garnet-biotite geothermometer. *Am. Mineral.* 85, 881–892.
- Holland, T.J.B., Blundy, J., 1994. Non-ideal interactions in calcic amphiboles and their bearing on amphibole-plagioclase thermometry. *Contrib. Mineral. Petrol.* 116, 433–447.
- Holland, T.J.B., Powell, R., 1998. An internally consistent thermodynamic dataset for phases of petrological interest. *J. Metam. Geol.* 16, 309–343.
- Holland, T.J.B., Powell, R., 2011. An improved and extended internally consistent thermodynamic dataset for phases of petrological interest, involving a new equation of state for solids. *J. Metam. Geol.* 29, 333–383.
- Htay, K.N., Aung, L.T., Tajcmanova, L., Heinrich, C.A., 2017. The evidences of high temperature-medium pressure, granulite grade metamorphism in Momeik Area, Mogok Metamorphic Belt, Myanmar. *Abstract Volume, 1st Myanmar Applied Earth Sciences Association 197*.
- Hughes, R.W., Manorotkul, W., Hughes, E.B., 2014. *Ruby & sapphire: a collector's guide*. GIT, Bangkok, 384 pp.
- Hughes, R.W., Manorotkul, W., Hughes, E.B., 2017. *Ruby & sapphire: a gemmologists guide*. Lotus Publishing 816 pp.
- Hughes, R.W., 1997. *Ruby & sapphire*. Boulder, CO, RWH Publishing, 512 pp.
- Iyer, L.A.N., 1953. *The Geology and Gemstones of the Mogok Stone Tract, Burma* 100 pp.
- Kozioł, A.M., Newton, R.C., 1988. Redetermination of the anorthite breakdown reaction and improvement of the plagioclase-garnet-Al₂SiO₅-quartz geobarometer. *Am. Mineral.* 73, 216–223.
- Kretz, R., 1983. Symbols of rock-forming minerals. *Am. Mineral.* 68, 277–279.
- La Touche, T.H.D., 1913. *Geology of the Northern Shan State*. Office of the Geological Survey of India, Calcutta, India, 39, Part 2, 379 pp.
- Lal, R.K., 1993. Internally consistent recalibrations of mineral equilibria for geothermobarometry involving garnet-orthopyroxene-plagioclase-quartz assemblages and their application to the South Indian granulites. *J. Metam. Geol.* 11, 855–866.
- Le Bas, M.J.L., Maitre, R.W.L., Streckeisen, A., Zanettin, B., 1986. A chemical classification of volcanic rocks based on the total alkali-silica diagram. *J. Petrol.* 27, 745–750.
- Leake, B.W., Woolley, A.R., Arps, C.E.S., Birch, W.D., Gilbert, M.C., Grice, J.D., Hawthorne, F.C., Kato, A., Kisch, H.J., Krivovichev, V.G., Linthout, K., Laird, J., Mandarino, J., Maresch, W.V., Nickel, E.H., Rock, N.M.S., Schumacher, J.C., Smith, D.C., Stephenson, N.C.N., Ungaretti, L., Whittaker, E.J.W., Youzhi, G., 1997. Nomenclature of amphiboles. Report of the subcommittee on amphiboles of the International Mineralogical Association Commission on new minerals and mineral names. *Eur. J. Mineral.* 9, 623–651.
- Lee, H.Y., Chung, S.L., Yang, H.M., 2016. Late Cenozoic volcanism in central Myanmar: geochemical characteristics and geodynamic significance. *Lithos* 245, 174–190.
- Licht, A., France-Lanord, C., Reisberg, L., Fontaine, C., Soe, A.N., Jaeger, J.-J., 2013. A paleo Tibet-Myanmar connection? Reconstructing the Later Eocene drainage

- systems of Central Myanmar using a multi-proxy approach. *J. Geol. Soc. London* 170, 929–939.
- Lindsley, D.H., 1983. Pyroxene thermometry. *Am. Mineral.* 68, 477–493.
- Lustrino, M., Fedele, L., Agostini, S., Prelević, D., Salari, G., 2019. Leucites within and around the Mediterranean area. *Lithos* 324–325, 216–233.
- Metcalf, I., 2013. Gondwana dispersion and Asian accretion: tectonic and palaeogeographic evolution of eastern Tethys. *J. Asian Earth Sci.* 66, 1–33.
- Miller, C., Thoni, M., Frank, W., Grasmann, B., Klotzli, U., Guntli, P., Draganits, E., 2001. The early Palaeozoic magmatic event in the Northwest Himalaya, India: source, tectonic setting and age of emplacement. *Geol. Mag.* 138, 237–251.
- Mitchell, A.H.G., 1993. Cretaceous-Cenozoic tectonic events in the western Myanmar (Burma)-Assam region. *J. Geol. Soc. London* 150, 1089–1102.
- Morimoto, N., Fabries, J., Ferguson, A.K., Ginzburg, I.V., Ross, M., Seifert, F.A., 1988. Nomenclature of pyroxenes. *Mineral. Petrol.* 39, 55–76.
- Moyd, L., 1949. Petrology of the nepheline and corundum rocks of southeastern Ontario. *Am. Mineral.* 34, 736–750.
- Müller, D., Franz, L., Herzig, P., Hunt, S., 2001. Potassic igneous rocks from the vicinity to epithermal gold mineralization at Lihir Island, Papua New Guinea. *Lithos* 57, 163–186.
- Newton, R.C., Aranovich, L.Y., Hansen, E.C., Vandenhuevel, B.A., 1998. Hypersaline fluids in Precambrian deep-crustal metamorphism. *Precamb. Res.* 91, 41–63.
- Pearce, J.A., Parkinson, L.J., 1993. Trace element models for mantle melting: application to volcanic arc petrogenesis. In Prichard, H.M., Alabaster, T., Harris, N.B.W., Neary, C.R. (Eds.), *Magmatic Processes and Plate Tectonics*. Geological Society Special Publications 76, 373–403.
- Phyo, M.M., Franz, L., Bieler, E., Balmer, W., Krzemnicki, M.S., 2019. Spinel from Mogok, Myanmar – A detailed inclusion study by Raman microspectroscopy and scanning electron microscopy. *J. Gemmol.* 36, 418–435.
- Phyo, M.M., Wang, H.A.O., Guillong, M., Berger, A., Franz, L., Balmer, W., Krzemnicki, M.S., 2020. U-Pb dating of zircon and zirconolite inclusions in marble-hosted gem-quality ruby and spinel from Mogok, Myanmar. *Minerals* 10, 195.
- Powell, M., Powell, R., 1977. A nepheline-alkali feldspar geothermometer. *Contrib. Miner. Petrol.* 62, 193–204.
- Prelević, D., Akal, C., Romer, R.L., Mertz-Kraus, R., Helvacı, C., 2015. Magmatic response to slab tearing: constraints from the Afyon Alkaline Volcanic Complex, Western Turkey. *J. Petrol.* 56, 527–562.
- Richards, A., Argles, T., Harris, N., Parrish, R., Ahmad, T., Darbyshire, F., Draganits, E., 2005. Himalayan architecture constrained by isotopic tracers from clastic sediments. *Earth Planet. Sci. Lett.* 236, 773–796.
- Rickwood, P.C., 1989. Boundary lines within petrologic diagrams which use oxides of major and minor elements. *Lithos* 22, 247–263.
- Romer, R.L., Förster, H.-J., Breikreuz, C., 2001. Intracontinental extensional magmatism with a subduction fingerprint: the late Carboniferous Halle Volcanic Complex (Germany). *Contrib. Miner. Petrol.* 141, 201–221.
- Romer, R.L., Hahne, K., 2010. Life of the Rheic Ocean: Scrolling through the shale record. *Gondw. Res.* 17, 236–253.
- Romer, R.L., Heinrich, W., Schröder-Smeibidl, B., Meixner, A., Fischer, C.-O., Schulz, C., 2005. Elemental dispersion and stable isotope fractionation during reactive fluid-flow and fluid immiscibility in the Bufa del Diente aureole, NE-Mexico: Evidence from radiographies and Li, B, Sr, Nd, and Pb isotope systematics. *Contrib. Miner. Petrol.* 149, 400–429.
- Romer, R.L., Meixner, A., Hahne, K., 2014. Lithium and boron isotopic composition of sedimentary rocks – the role of source history and depositional environment: a 250 Ma record from the Cadomian orogeny to the Variscan orogeny. *Gondw. Res.* 26, 1093–1110.
- Ryburn, R.J., Raheim, A., Green, D.H., 1976. Determination of P, T paths of natural eclogites; a correction. *Lithos* 9, 161–164.
- Santosh, M., Omori, S., 2008. CO₂ flushing: a plate tectonic perspective. *Gondw. Res.* 13, 86–102.
- Searle, M.P., Waters, D.J., Morley, C.K., Gardiner, N.J., Htun, U.K., Nu, T.T., Robb, L.J., 2017. Chapter 12 Tectonic evolution of the Mogok metamorphic and Jade mines belts and ophiolitic terranes of Burma (Myanmar). *Myanmar: Geology, Resources and Tectonics* (Vol. 48). Geological Society Memoir 48, 261–293.
- Searle, D.L., Haq, B.T., 1964. The Mogok belt of Burma and its relationship to the Himalayan orogeny. *Int. Geol. Congr.* 22, 132–161.
- Searle, M.P., Noble, S.R., Cottle, J.M., Waters, D.J., Mitchell, A.H.G., Hlaing, T., Horstwood, M.S.A., 2007. Tectonic evolution of the Mogok metamorphic belt, Burma (Myanmar) constrained by U-Th-Pb dating of metamorphic and magmatic rocks. *Tectonics* 26, TC2083.
- Searle, M.P., Garber, J.M., Hacker, B.R., Htun, U.K., Gardiner, N.J., Waters, D.J., Robb, L. J., 2020. Timing of syenite-charnockite magmatism and ruby and sapphire metamorphism in the Kogok Valley Region, Myanmar. *Tectonics* 39.
- Sone, M., Metcalfe, I., 2008. Parallel Tethian sutures in mainland South-East Asia: New insights for Palaeo-Tethys closure and implications for the Indosinian Orogeny. *C. R. Geoscience* 340, 166–179.
- Spear, F.S., 1993. *Metamorphic phase equilibria and pressure-temperature-time paths*. Mineralogical Society of America Monographs, 799 pp.
- Sutherland, F.L., Zaw, K., Meffre, S., Thompson, J., Goemann, K., Thu, K., Nu, T.T., Zin, M.M., Harris, S.J., 2019. Diversity in ruby geochemistry and its inclusions: intra- and inter-continental comparisons from Myanmar and Eastern Australia. *Minerals* 9, 28.
- Tajčmanová, L., Konopasek, J., Schulmann, K., 2006. Thermal evolution of the orogenic lower crust during exhumation within a thickened Moldanubian root of the Variscan belt of central Europe. *J. Metam. Geol.* 24, 119–134.
- Themelis, T., 2008. *Gems and Mines of Mogok*, 352 pp.
- Thu, K., Enami, M., 2018. Evolution of metamorphic fluid recorded in granulite facies metacarbonate rocks from the middle segment of the Mogok metamorphic belt in central Myanmar. *J. Metam. Geol.* 36, 905–931.
- Thu, Y.K., Win, M.M., Enami, M., Tsuboi, M., 2016. Ti-rich biotite in spinel and quartz-bearing paragneiss and related rocks from the Mogok metamorphic belt, central Myanmar. *J. Mineral. Petrol. Sci.* 111, 270–282.
- Thu, Y.K., Enami, M., Kato, T., Tsuboi, M., 2017. Granulite facies paragneisses from the middle segment of the Mogok metamorphic belt, central Myanmar. *J. Mineral. Petrol. Sci.* 112, 1–19.
- Thu, K., 2007. *The igneous rocks of the Mogok Stone Tract: their distribution, petrography, petrochemistry, sequence, geochronology and economic geology*. Ph.D. Thesis, University of Yangon, Myanmar.
- Touret, J.L.R., 1971. Le faciès granulite en Norvège Méridionale. II: les inclusions fluides. *Lithos* 4, 423–436.
- Touret, J.L.R., Huizenga, J.M., 2012. Fluid-assisted granulite metamorphism: a continental journey. *Gondw. Res.* 21, 224–235.
- Waltham, T., 1999. The ruby mines of Mogok. *Geol. Today* 15, 143–149.
- White, R.W., Powell, R., Holland, T.J.B., 2007. Progress relating to calculation of partial melting equilibria for metapelites. *J. Metamorphic Geol.* 25, 511–527.
- White, R.W., Powell, R., Holland, T.J.B., Johnson, T.E., Green, E.C.R., 2014a. New mineral activity-composition relations for thermodynamic calculations in metapelitic systems. *J. Metamorphic Geol.* 32, 261–286.
- White, R.W., Powell, R., Johnson, T.E., 2014b. The effect of Mn on mineral stability in metapelites revisited: new a-x relations for manganese-bearing minerals. *J. Metamorphic Geol.* 32, 809–828.
- Win, M.M., Enami, M., Kato, T., 2016. Metamorphic conditions and CHIME monazite ages of Late Eocene to Late Oligocene high-temperature Mogok metamorphic rocks in central Myanmar. *J. Asian Earth Sci.* 117, 304–316.
- Wu, C.-M., Zhang, J., Ren, L.D., 2004. Empirical garnet-biotite-plagioclase-quartz (GBPQ) geobarometry in medium- to high-grade metapelites. *J. Petrol.* 45, 1907–1921.
- Xiang, H., Zhang, L., Zhong, Z.-Q., Santosh, M., Zhou, H.-W., Zhang, H.-F., 2012. Ultrahigh-temperature metamorphism and anticlockwise P-T path of Paleozoic granulites from north Qinling-Tongbai orogen, Central China. *Gondw. Res.* 21, 559–576.
- Yonemura, K., Osanail, Y., Zaw, T.N., Nakano, N., Charusiri, P., Adachi, T., 2013. EPMA U-Th-Pb monazite dating of metamorphic rocks from the Mogok Metamorphic Belt, central Myanmar. *J. Mineral. Petrol. Sci.* 108, 184–188.
- Zartman, R.E., Doe, B.R., 1981. Plumbotectonics - the model. *Tectonophysics* 75, 135–162.
- Zaw, K., 1989. Comments on transcurrent movements in the Myanmar-Andaman sea region. *Geology* 17, 93–95.
- Zaw, K., 1990. Geological, petrological and geochemical characteristics of granitoid rocks in Burma: with special reference to the associated W-Sn mineralization and their tectonic setting. *J. SE Asian Earth Sci.* 4, 293–335.
- Zaw, K., 1998. Geological evolution of selected granitic pegmatites in Myanmar (Burma): constraints from regional setting, lithology, and fluid inclusion studies. *Int. Geol. Rev.* 40, 647–662.
- Zaw, K., Sutherland, F.L., Graham, I., Meffre, S., Thu, K., 2010. Dating zircon inclusions in gem corundum deposits and genetic implications. *Proceedings of the 13th Quadrennial IAGOD Symposium, Adelaide, Australia*, 7.
- Zaw, K., Thu, K., Meffre, S., Yui, T.F., Sutherland, F.L., 2015. Vanadium-rich ruby and sapphire within Mogok Gemfield, Myanmar: implications for gem color and genesis. *Miner. Deposita* 50, 25–39.
- Zaw, K., Swe, K., Barber, A.J., Crow, M.J., Nwe, Y.Y., 2017. Introduction to the geology of Myanmar. In: Barber, A.J., Zaw, K., Crow, M.J. (Eds.), *Myanmar: Geology, Resources and Tectonics*, Chapter 1. Geological Society London Memoirs, pp. 1–17.
- Zaw, K., 2017. Overview of mineralization styles and tectonic-metallogenic setting in Myanmar. In: Barber, A.J., Zaw, K., Crow, M.J. (Eds.), *Myanmar: Geology, Resources and Tectonics*, Chapter 24. Geological Society London Memoirs, 531–556.

Further reading

- Downs, R.T., 2006. The RRUFF Project: an integrated study of the chemistry, crystallography, Raman and infrared spectroscopy of minerals. In: *Program and Abstracts of the 19th General Meeting of the International Mineralogical Association in Kobe, Japan*, 003-13.
- Zuleger, E., Erzinger, J., 1988. Determination of the REE and Y in silicate materials with ICP-AES. *Fresenius' Zeitschrift für Analytische Chemie* 332, 140–143.